Current Address:
T-8 Green Park (Main)
New Delhi 110016, India
+91-8826535608

Amos Greene Winter, V

awinter@mit.edu
www.amoswinter.com

Permanent Address:
126 Pinnacle Springs Rd.
Chesterfield, NH 03443
+1-617-312-4207

RESEARCH INTERESTS

Biologically-inspired design; design for emerging markets; design for international development; cross-cultural technology transfer; fluid, solid, granular mechanics; medical device design; biomechanics; mechanical, precision machine design; design of ocean systems; machine-soil interactions.

TEACHING INTERESTS

Mechanical, precision machine design; technology for emerging markets; international development and appropriate technology; disability and assistive devices; statics and solid mechanics; manufacturing processes.

EDUCATION

Massachusetts Institute of Technology — Cambridge, MA
Ph.D., Mechanical Engineering (GPA 4.7/5.0) — Sept. 2005-Sept. 2010
Thesis: "Biologically inspired mechanisms for burrowing in undersea substrates"

Massachusetts Institute of Technology — Cambridge, MA
S.M., Mechanical Engineering (GPA 4.6/5.0) — Sept. 2003-June 2005
Thesis: "Design of fluid film journal bearings containing continuous 3D fluid pathways which are formed by wrapping a sheet containing 2D through-cut features"

Tufts University — Medford, MA
B.S., Mechanical Engineering, *Magna Cum Laude* (GPA 3.74/4.0) — Sept. 1999-June 2003
Thesis: "JUMBOt: A robot to compete on Battle Bots"

University of Canterbury — Christchurch, New Zealand
Semester Abroad — Feb.-June 2003

RESEARCH EXPERIENCE

Singapore University of Technology and Design (SUTD) – MIT International Design Center — Singapore
Post-Doctoral Research Associate - Supervisor: Prof. Daniel Frey — Sept. 2010-Present
MIT Department of Mechanical Engineering — Cambridge, MA
Research Affiliate — Sept. 2010-Present
Indian Institute of Technology Delhi — New Delhi, India
Visiting Researcher - Supervisor: Prof. Sudipto Mukherjee — Sept. 2010-Present
MIT Mobility Lab (M-Lab) — Cambridge, MA
Project lead - Leveraged Freedom Chair (http://mlab.mit.edu/lfc) — Feb. 2008-Present

- Invented, field trialed, and disseminated the Leveraged Freedom Chair (LFC), a novel mobility aid designed for high efficiency and all-terrain performance that can be made and repaired anywhere in the world (topic of postdoc).
- Invented a single-speed, variable mechanical advantage lever-propelled drivetrain that effectively changes gear by varying hand position on the levers. Made from local bike parts and yields a 3:1 change in mechanical advantage.
- Researched human upper body strength, power, and kinematic capabilities for mobility aid propulsion; combined with understanding of local terrain to deterministically design drivetrain geometry for optimal performance.
- Tested eight alpha prototypes in East Africa with fulltime wheelchair users, measured performance advantages compared to existing mobility products.
- Collaborated with African and Guatemalan stakeholders and wheelchair manufacturers to design a beta prototype with 30% reduced weight, 3.5" reduced width, and improved stability performance. Beta LFC under trial in Guatemala.
- Partnered with BMVSS Jaipur Foot (biggest assistive device provider in world) and IIT Delhi on pre-production trial,

biomechanical testing, and commercialization of the LFC in India.
- Led collaboration between Continuum (multinational product design firm), MIT Sloan School of Management students, and MIT engineers to create and sell a first-world LFC to subsidize developing world chairs.

MIT Department of Mechanical Engineering Cambridge, MA
Ph.D. Research Assistant, Hosoi Research Group - Advisor: Prof. Anette "Peko" Hosoi June 2006-Sept. 2010
Ph.D. Research Assistant, Precision Engineering Research Group - Advisor: Prof. Alex Slocum Feb. 2007-Sept. 2010
- Identified burrowing and anchoring biological mechanisms to be modeled, optimized, and implemented in lightweight, low-power engineering and military applications (topic of Ph.D. thesis).
- Invented, designed, and constructed a testing apparatus to visualize sub-sea organisms burrowing in real time.
- Discovered that razor clams locally fluidize the substrate around their shell to decrease drag while burrowing.
- Determined digging mechanisms employed by razor clams are more efficient than current engineering systems.
- Modeled soil/fluid/solid mechanics at play during localized fluidization, determined properties of fluidized zone can be predicted from two common geotechnical parameters: coefficient of lateral earth pressure and friction angle.
- Collaborated with Prof. Wolfgang Losert at the University of Maryland to verify localized fluidization theory in 3D.
- Invented, designed, and constructed RoboClam, a biologically-inspired robotic burrowing device that utilizes localized soil fluidization to achieve the same digging performance and energetic savings as razor clams.
- Tested RoboClam in both idealized granular and real marine substrates, verified localized fluidization works in both granular and cohesive soils.

Massachusetts General Hospital Boston, MA
Consultant - Advisor: Dr. Timothy Bhattacharyya, Orthopaedic Surgeon Jan. 2006-Jan. 2008
- Devised a non-invasive femur fracture criterion to predict bone stresses during hip replacement surgery.
- Developed a bone testing apparatus to measure bone fracture stress and verify the femur fracture criterion.

MIT Department of Mechanical Engineering Cambridge, MA
S.M. Research Assistant, Precision Compliant Systems Lab - Advisor: Prof. Martin Culpepper Sept. 2003-Jan. 2006
- Invented a process for making fluid film bearings without precision machining at 1/10 the cost of conventional bearings by wrapping thin sheets of material with through-cut features (topic of S.M. thesis).
- Investigated the use of carbon nanotubes as flexural elements to increase range of motion in nano/micro machines.
- Collaborated with Schlumberger to design compliant mechanisms for more reliable, low-cost oil well tools.
- Designed a 3-DOF flexure stage with a dynamic error motion reducing topology for a DNA scanning microscope.
- Created the "Floating Ball Universal Joint," a universal joint without pins that can be made with 2D cutting processes.

ADVISING EXPERIENCE

N. Scolnik, MIT Undergraduate Thesis, Mechanical Engineering Jan. 2010-May 2010
M. Bollini, MIT Undergraduate Thesis, Mechanical Engineering Jan. 2009-May 2009
A. Maguire, MIT Undergraduate Thesis, Mechanical Engineering Jan. 2009-May 2009
C. Jones, MIT Undergraduate Thesis, Mechanical Engineering Sept. 2008-May 2009
C. Becker, MIT Undergraduate Thesis, Mechanical Engineering Jan. 2008-May 2008
N. Wang, MIT Undergraduate Thesis, Mechanical Engineering Sept. 2007-May 2008
L. Todman, Cambridge University, UK, Undergraduate Thesis, Mechanical Engineering Sept. 2007-May 2008
B. Judge, MIT Undergraduate Research Opportunities Program June 2009-Present
D. Dorsch, MIT Undergraduate Research Opportunities Program May 2009-Present
R. Deits, MIT Undergraduate Research Opportunities Program Jan. 2009-Present
D. DeLatte, MIT Undergraduate Research Opportunities Program June 2008-Present
H. O'Hanley, MIT Undergraduate Research Opportunities Program June 2008-Present
A. Lehto, MIT Undergraduate Research Opportunities Program June 2010-Aug. 2010
X. Chen, MIT Undergraduate Research Opportunities Program Sept. 2009-May 2010
L. Schuhrke, MIT Undergraduate Research Opportunities Program Sept. 2009-Dec. 2009
N. Bhartiya, MIT Undergraduate Research Opportunities Program Oct. 2009-Dec. 2009
J. Walton, MIT Undergraduate Research Opportunities Program June 2009-Aug. 2009
D. Whited, MIT Undergraduate Research Opportunities Program June 2009-Aug. 2009

K. Ray, MIT Undergraduate Research Opportunities Program — Jan. 2009-May 2009
F. Funnel, MIT Undergraduate Research Opportunities Program — Sept. 2008-May 2009
T. Scolnik, MIT Undergraduate Research Opportunities Program — Sept. 2007-May 2008
S. Duffley, MIT Undergraduate Research Opportunities Program — Feb. 2008-June 2007
M. Bollini, MIT Undergraduate Research Opportunities Program — Sept. 2006-May 2007
S. Sovero, MIT Undergraduate Research Opportunities Program — Sept. 2005-Dec. 2005
C. Walker, MIT Undergraduate Research Opportunities Program — June 2004-Dec. 2004
J. Sadler, MIT Undergraduate Research Opportunities Program — Mar. 2004-Dec. 2004
K. Harrison, MIT Undergraduate Research Opportunities Program — Feb. 2004-Aug. 2004

TEACHING EXPERIENCE

Massachusetts Institute of Technology — Cambridge, MA
Lecturer and Lab Instructor, SP.784 "Wheelchair Design in Developing Countries" — Feb.-May 2007-2010

- Developed and implemented a full course curriculum to teach about the issues facing third-world disabled.
- Collaborated with 14 wheelchair manufacturers in developing countries and wheelchair experts in the US and Europe.
- Arranged multidisciplinary student teams to conduct projects on topics such as hardware design, manufacturing optimization, biomechanics modeling, and business plan development.
- Organized guest lecturers from MIT Faculty, wheelchair experts, and manufacturers from developing countries.
- Established summer fellowships with the MIT Public Service Center and Undergraduate Research Opportunities Program for students to implement class projects into partner manufacturer workshops.
- Designed and maintained course website (http://web.mit.edu/sp.784/www/)
- Lab instructor for project team that improved biomechanics of handcycle propulsion (2007).
- Lab instructor for project team that developed a folding 3-wheeled wheelchair (2008).
- Lab instructor for project team that created a powered-assisted handcycle (2009).
- Lab instructor for project team refining elements of the Leveraged Freedom Chair (2010).

St. Paul's School Advanced Studies Program — Concord, NH
Master Teacher, Introduction to Engineering class — June-Aug. 2006, 2007

- Developed full course curriculum including a term-long underwater robot project, daily lectures, field trips, demonstrations, lab experiments, and homework problems to teach engineering fundamentals to high school students.
- Supervised four interns, built and maintained a course website (http://web.mit.edu/awinter/www/ASPIE/index.html), and organized individual robot kits for 12 students.

Massachusetts Institute of Technology — Cambridge, MA
Teaching Assistant, 2.002 "Mechanics and Materials II" — Feb.-May 2006

- Instructed lab experiments, led review sessions, composed homework solutions, aided in lab design, wrote and graded test problems, and supervised three graders as part of teaching the fundamentals of material behavior.

Massachusetts Institute of Technology — Cambridge, MA
Teaching Assistant, 2.000 "How and Why Machines Work" — Feb.-May 2005

- Led four lectures on the physics of machines, developed a lesson on fuel cells, designed and supervised a term-long fuel cell project, distributed and maintained class tablet PCs, supervised lab sections, and graded class work.

Massachusetts Institute of Technology — Cambridge, MA
Team Mentor, 2.75 "Precision Machine Design" — Sept.-Dec. 2009

- Mentored a team that designed a high-efficiency, lever-driven wheelchair propelled by the pectoralis major and latissimus dorsi muscles.

University of Michigan — Ann Arbor, MI
Team Mentor, ME450 "Design and Manufacturing III" — Jan.-Apr. 2009

- Mentored a team that designed a folding hand-powered tricycle attachment for developing world wheelchairs.

Massachusetts Institute of Technology Cambridge, MA
Lab Instructor, 2.00b/SP.778 **"**Toy Product Design" Feb.-May 2006, 2008

- Advised a student team during the design of a toy/oral hygiene product (2006).
- Advised a student team during the design of a toy to demonstrate scientific principles (2008).

Massachusetts Institute of Technology Cambridge, MA
Lab Instructor, Trip Leader, 11.025/11.190/11.472/SP.721 "D-Lab: Development" Feb. 2007-Jan. 2008

- Coordinated class projects on international development and led student team to Tanzania.

St. Paul's School Advanced Studies Program Concord, NH
Intern, Artificial Intelligence class June-Aug. 2004

- Taught high school students about AI through programming assignments, engineering lessons, and hands-on projects.

Tufts University Medford, MA
Volunteer, Elementary School Engineering Outreach Program Jan. 2001-May 2003

- Taught basic engineering principles to elementary school children in Lincoln, MA, Malden, MA, and Christchurch, New Zealand.

INTERNATIONAL DEVELOPMENT

MIT Mobility Lab (M-Lab) Cambridge, MA
Founder and Director Dec. 2007-Present

- Founded M-Lab to develop high-risk, high-payoff mobility projects that that will make drastic improvements to wheelchair technology and the lives of disabled people.
- M-Lab offers a laboratory through which to conduct graduate and undergraduate research projects, a small workshop similar to ones found in the developing world, and travel grants to implement mobility technology.
- More information available at: http://mlab.mit.edu/

Engineering Manual for Wheelchair Technicians USA, Tanzania, Kenya, Zambia
Independent Fellow, MIT Public Service Center Fellowship Program June-Sept. 2006

- Authored a manual, "Mechanical Principles of Wheelchair Design," that uses hands-on examples to empower African wheelchair manufacturers with the knowledge to fix design problems and rely less on US/European technology.
- Distributed the manual to wheelchair technicians in Kenya, Tanzania, and Zambia.
- Manual is available for download (http://web.mit.edu/awinter/Public/Wheelchair/Wheelchair%20Manual-Final.pdf)

Assessment of Wheelchair Technology in Tanzania Tanzania
Independent Fellow, MIT Public Service Center Fellowship Program June-Aug. 2005
Intern, Whirlwind Wheelchair International

- Composed a report on the current state of wheelchair technology in Tanzania to give wheelchair builders, donators, and users feedback on the issues affecting the distribution and use of appropriate wheelchair technology.

PROFESSIONAL EXPERIENCE

Bluefin Robotics Corporation Cambridge, MA
Contractor, Autonomous underwater vehicle design Jan. 2006-June 2010

- Invented a novel two degree-of-freedom propulsion system with both actuators and thruster in a single rigid housing.
- Designed a compact, 4500m depth rated radio direction finder (RDF) beacon.
- Developed a variable buoyancy system to allow vehicles to operate in both salt and fresh water.
- Engineered an ultra-compact, 60lbs drop weight mechanism that enables vehicles to surface in emergency situations.
- Designed a "Zero Volume" lift point that utilizes vehicle shell strength and maximizes buoyancy volume.

Schlumberger-Doll Research Center Cambridge, MA
Intern, Design and testing of down-hole anchoring and tractoring systems Jan.-June 2006

- Derived governing equations and generated concepts to facilitate the design of compliant anchoring devices.
- Improved and tested an apparatus to measure and predict down-hole tractor and mud cake interaction.

Bluefin Robotics Corporation Cambridge, MA
Intern, Autonomous underwater vehicle design June-Aug. 2003

- Conceived and designed new mechanical systems including a retractable GPS antenna, an improved battery securing latch, a vehicle single point lift eye and internal frame, a hull drain valve, and a portable 15ft vehicle test tank.

NASA Jet Propulsion Laboratory Pasadena, CA
Intern, Mechanical and Robotics Technologies Group June-Aug. 2002

- Redesigned drive train components to improve top-speed and reliability for the "PackBot" urban combat robot.

Monterey Bay Aquarium Research Institute Moss Landing, CA
Intern, Underwater engineering June-Aug. 2001

- Built a LEGO RCX computer controlled underwater robot to be sold as a LEGO kit at the Monterey Bay Aquarium.

AWARDS

2010 Tufts University Young Alumni Distinguished Achievement Award	2011
Nominee, Brit Insurance Designs of the Year for the Leveraged Freedom Chair, Design Museum London	2011
R&D 100 Award for the Leveraged Freedom Chair, given by R&D Magazine for the 100 most technologically significant products of the year	2010
R&D 100 Editors' Choice Award for the Leveraged Freedom Chair, given to the three favorite R&D 100 award winners by the magazine's editors	2010
MIT School of Engineering Graduate Student Extraordinary Teaching and Mentoring Award, the highest honor given to a graduate student for teaching and mentoring at MIT	2010
ASME Innovation Showcase, 1st place for the Leveraged Freedom Chair	2010
Gold Award, Spark Awards for design, world changing category for the Leveraged Freedom Chair	2010
Winner, Scientific American's World Changing Ideas video contest for the Leveraged Freedom Chair	2010
Wall Street Journal Technology Innovation Awards, medical devices category, runner up for the Leveraged Freedom Chair	2010
National Collegiate Inventors and Innovators Alliance (NCIIA) Advanced E-Teams grant for Indian trial and dissemination of the Leveraged Freedom Chair	2010
Fulbright-Nehru Student Research Fellowship to India (declined)	2010
Finalist, Lemelson-MIT Student Prize	2010
Extraordinary Stories Award, National Academy of Engineering Grand Challenge Summit	2010
MIT Department of Mechanical Engineering deFlorez Award for Design, 3rd place for the Leveraged Freedom Chair	2010
Inter-American Development Bank, $50,000 World of Solutions grant for Leveraged Freedom Chair trial in Guatemala	2009
ASME IDETC Conference, Graduate Student Mechanism Design Competition, 1st place for the Leveraged Freedom Chair	2009
ASME IDETC Conference, Robot Design Competition, 2nd place for RoboClam	2009
RESNA Student Design Competition Finalist, for the Leveraged Freedom Chair	2009
MIT Department of Mechanical Engineering deFlorez Award for Technology Innovation/Invention, 2nd place for RoboClam	2009
MIT IDEAS Competition Winner, Award for International Technology for the Leveraged Freedom Chair	2008
Hugh Hampton Young Memorial Fund Fellowship	2007-2009
National Collegiate Inventors and Innovators Alliance (NCIIA) Course Grant for Wheelchair Design in Developing Countries Class	2007
MIT Alumni Sponsored Funding Opportunities Grant for Wheelchair Design in Developing Countries class	2006
MIT Public Service Center Independent Fellowship	2006

MIT Public Service Center Independent Fellowship	2005
NSF Graduate Research Fellowship Honorable Mention	2005
MIT 2.810 "Manufacturing Processes and Systems" RC Car Race Winner	2004
Tufts Alex Elias Memorial Prize Scholarship	2003
Tufts Varsity Football Letter Winner	2001, 2002

PATENTS

1. Winter V, A.G., et al. "Wheelchair with Lever Drivetrain." Patent application no. 12914986, Steptoe and Johnson LLP, Utility filed October 28, 2010.
2. Winter V, A.G., et al. "Method and Apparatus for Penetrating Particulate Substrates." Patent application no. 12455392, Hamilton, Brook, Smith & Reynolds, P.C. Utility filed June 1, 2009.

PUBLICATIONS

1. A.G. Winter, V, et al. "The design and manufacturing of a lever-propelled, all-terrain wheelchair for developing countries," 2011. (in preparation, to be submitted to the *Journal of Mechanical Design*).
2. A.G. Winter, V, et al. "The design and *in situ* performance of a single speed, variable mechanical advantage drivetrain for developing country wheelchairs," 2011. (in preparation, to be submitted to the *Journal of Mechanical Design*)
3. A.G. Winter, V., et al. "Reinventing the wheelchair in the developing world," 2011. (in preparation, to be submitted to *Science*)
4. A.G. Winter, V., R.L.R. Deits, D.L. Dorsch, A.E. Hosoi, A.H. Slocum. "The design, testing, and performance of a burrowing robot inspired by the digging mechanisms of Atlantic razor clams," 2011. (in preparation, to be submitted to the *Journal of Mechanical Design*)
5. A.G. Winter, V., L. Jacob, R.L.R. Deits, A.E. Hosoi, W. Losert. "The mechanics of localized fluidization burrowing," 2011. (in preparation, to be submitted to *Physical Review E*)
6. A.G. Winter, V., R.L.R. Deits, D.L. Dorsch, A.E. Hosoi, A.H. Slocum. "Razor Clam to RoboClam: Burrowing Drag Reduction Mechanisms and their Robotic Adaptation," 2011. (in preparation, to be submitted to *The Proceedings of the National Academy of Sciences*)
7. A.G. Winter, V., A.E. Hosoi. "Localized fluidization burrowing mechanics of *Ensis directus*," 2011 (submitted to *The Journal of Experimental Biology*)
8. A.G. Winter, V., R.L.R. Deits, D.L. Dorsch, A.E. Hosoi, A.H. Slocum. "Identification and Evaluation of *Ensis directus* for Biologically-inspired Subsea Burrowing Systems," 2011. (in press, *The Journal of Integrative and Comparative Biology*)
9. S. Jung, A.G. Winter, V., A.E. Hosoi. "Dynamics of animals digging into wet soil," 2010. (in press, *International Journal of Nonlinear Mechanics*)
10. A.G. Winter, V. *Biologically Inspired Mechanisms for Burrowing in Undersea Substrates.* Ph.D. Thesis, MIT Department of Mechanical Engineering, September 2010.
11. A.G. Winter, V, et al. "Teaching RoboClam to Dig: The Design, Testing, and Genetic Algorithm Optimization of a Biomimetic Robot." IEEE IROS 2010. Paper # WeET11.3, 2010 (paper and oral presentation)
12. A.G. Winter, V, et al. "The design, fabrication, and performance of the East African trial Leveraged Freedom Chair." ASME IDETC 2010. Paper# DETC2010-29096. (paper and oral presentation)
13. A.G. Winter, V, et al. "Multi-substrate burrowing performance and constitutive modeling of RoboClam: a biomimetic robot based on razor clams." ASME IDETC 2010. Paper# DETC2010-29060. (paper and presentation)
14. A.G. Winter, V, et al. "The Design and Fabrication of the East African Trial Leveraged Freedom Chair," 2010 RESNA Conference. (paper and oral presentation)
15. A.G. Winter, V, et al. "The design and testing of a low-cost, globally-manufacturable, multi-speed mobility aid designed for use on varied terrain in developing and developed countries." ASME IDETC 2009. Paper# DETC2009-86808. (paper, oral presentation, student design competition poster)
16. A.G. Winter, V, et al. "The Design and Testing of RoboClam: A Machine used to Investigate and Optimize Razor Clam-Inspired Burrowing Mechanisms for Engineering Applications." ASME IDETC 2009. Paper# DETC2009-87609. (paper, oral presentation, student design competition poster)
17. A.G. Winter, V, et al. "The Leveraged Freedom Chair: A Wheelchair Designed for Developing Countries." Student Design Competition, 2009 RESNA Conference. (extended abstract and poster presentation)

18. A.G. Winter, V, et al. "The Leveraged Freedom Chair: A Wheelchair Designed for Developing Countries." 2009 RehabMove Conference. (extended abstract and poster presentation)
19. A.G. Winter. "A Serendipitous Passion: How a Public Service Center fellowship got me hooked on international development." Technology Review May/June 2008. http://www.technologyreview.com/article/20633/page1/
20. A.G. Winter, A.B. Smith. "Assessing MAARDEC: A Comparison with Other Assistive Device Workshop and Disability Organization Models (*Innovations Case Discussion*: MAARDEC)." Innovations Vol. 3 No. 3 (Summer 2008): 79-81. http://www.mitpressjournals.org/doi/pdfplus/10.1162/itgg.2008.3.3.79
21. A.G. Winter, V. "Assessment of Wheelchair Technology in Tanzania." *International Journal for Service Learning in Engineering* Vol. 2 No. 1 (Sept. 2006): 66-77.
22. A.G. Winter, V, R. Hotchkiss. "Mechanical Principles of Wheelchair Design." 2006.
23. A.G. Winter, V. *Design of fluid film journal bearings containing continuous 3D fluid pathways which are formed by wrapping a sheet containing 2D through-cut features.* Masters Thesis, MIT Department of Mechanical Engineering, June 2005.
24. S.E. Szczesny, A.G. Winter, V. "Design of a Gimbaled Compliant Mechanism Stage for Precision Motion and Dynamic Control in Z, θX & θY Directions." ASME DETC 2004. (paper and oral presentation)

INVITED TALKS

1. "Razor Clam to RoboClam: Biologically Inspired Mechanisms for Subsea Burrowing," Society for Integrative and Comparative Biology (SICB) annual meeting, Bioinspiration: Applying Mechanical Design to Experimental Biology symposium, Jan. 3, 2011.
2. "Design and Implementation of the Leveraged Freedom Chair: Innovating and Commercializing Appropriate Technology." Indian Institute of Technology Delhi, Department of Mechanical Engineering, Innovation Training Workshop, Dec. 13, 2010.
3. "Razor Clam to RoboClam: Burrowing Drag Reduction Mechanisms and their Robotic Adaptation," The Robotics Institute, Carnegie Mellon University, Foundations of Robotics Seminar, Nov. 10, 2010.
4. "Design and Implementation of the Leveraged Freedom Chair: Example of Commercializing Appropriate Technology," Lemelson Foundation Recognition and Mentoring Program summit, Indonesia, Oct. 29, 2010.
5. "The Leveraged Freedom Chair and Technology in the Developing World," Future of Technology Conference, Taubman College of Architecture and Urban Planning, University of Michigan, Sept. 24, 2010.
6. "The MIT Mobility Lab and the Leveraged Freedom Chair (LFC)," ASME Engineering for the Developing World Summit, National Academy of Sciences, Mar. 16, 2010.
7. "The Leveraged Freedom Chair: A Developing Country Wheelchair," World Health Innovation and Technology Congress, Extremely Affordable Health Innovations, Nov. 10, 2009.
8. "Biologically-Inspired Methods for Burrowing and Anchoring into Undersea Substrates," Tufts University Department of Mechanical Engineering Seminar Series, Oct. 29, 2009.
9. "Biologically-Inspired Mechanisms for Burrowing and Anchoring in Undersea Substrates," Naval Underwater Warfare Center, weekly seminar series, July 6, 2009.
10. "Projects and programs from the MIT Mobility Lab," Young Leaders for Social Change section, Unite for Sight Global Health and Innovation Summit, Yale University, April 18, 2009.
11. "Biologically Inspired Mechanisms for Burrowing and Anchoring," poster presentation and RoboClam demonstration, Battelle Board of Directors Annual Meeting, Columbus, OH, Feb. 4, 2009.
12. "Wheelchair Programs at MIT," Pan African Wheelchair Builders Association Congress, Moshi, Tanzania, September 19, 2007.
13. "Biologically Inspired Mechanisms for Burrowing and Anchoring," poster presentation, Battelle National Security Division Internal R&D Conference, Columbus, OH, June 13, 2007.
14. "Wheelchair Design in Developing Countries," Friday Speaker Series at the Sustainable International Development Programs, Heller School for Social Policy and Management, Brandeis University, February 16, 2007.
15. "Redesigning the Wheelchair," presentation at the MIT International Development Forum, April 24, 2006.
16. "Robots that operate in extreme environments: deep sea AUVs and BattleBots," presentation for elementary school students at Camp Robotech, Nashua, NH, August 6, 2003.
17. Guest speaker during Access Exeter, a summer program for high school students, Cambridge, MA, June 25, 2003.
18. "Using LEGOs to Teach Engineering Principles to Elementary School Students," Elementary school teacher training at the Monterey Bay Aquarium Research Institute, Moss Landing, CA, June 28, 2001.

PRESENTATIONS AND POSTERS

1. A.G. Winter, V, et al. "The design, testing, and performance of RoboClam, a robot inspired by the burrowing mechanisms of Atlantic razor clams (*Ensis directus*)," presentation, 62nd Annual Meeting of the American Physical Society Division of Fluid Dynamics, Minneapolis, MN, November 22, 2009.
2. A.G. Winter, V, A.E. Hosoi, "Drag reducing fluidization mechanisms employed by burrowing razor clams (*Ensis directus*)," poster presentation, Dynamics Days 2009, San Diego, CA, January 10, 2009.
3. A.G. Winter, V, A.E. Hosoi, "Drag reduction mechanisms employed by burrowing razor clams (*Ensis directus*)," presentation, 61st Annual Meeting of the American Physical Society Division of Fluid Dynamics, San Antonio, TX, November 23, 2008.
4. A.G. Winter, V, et al. "Leveraged Freedom Chair: A Wheelchair Designed for Developing Countries," poster presentation, Bioengineering Applications to Address Global Heath, Duke University, November 6-7, 2008.
5. A.G. Winter, V. "Biologically Inspired Mechanisms for Burrowing and Anchoring in Soft Undersea Substrates," poster presentation, A Day of Locomotion, Harvard University, October 16, 2007.
6. A.G. Winter, V. "Wheelchair Design in Developing Countries," presentation at the MIT Small-Talks Student Seminar Series, October 4, 2006.
7. A.G. Winter, V. "Fluid Film Bearings Requiring No Precision Machining Processes, Formed by Wrapping 2D sheets," poster presentation, ASPE 19th Annual Meeting 2004.
8. A.G. Winter, V. "Building a LEGO ROV using the Mindstorms Robotics Kit," Monterey Bay Aquarium Research Institute intern presentations, Moss Landing, CA, August 23, 2001.

ORGANIZATION MEMBERSHIP

Society for Integrative and Comparative Biology	2010-Present
American Physical Society	2009-Present
Rehabilitation Engineering and Assistive Technology Society of North America	2009-Present
American Society of Precision Engineering	2004-Present
American Society of Mechanical Engineers	2004-Present
Sigma Xi: The Scientific Research Society	2004-Present
Tau Beta Pi Engineering Honor Society	2003-Present

ACADEMIC ACTIVITIES

NSF Workshop: Research in Materials and Manufacturing for Extreme Affordability (RIMMEA)	Mar. 2011
ASME Engineering for Global Development Initiative Steering Committee	2011-Present
ASME Engineering for Change Advisory Committee	2010-Present
ASME Engineering for the Developing World Summit	Mar. 2010
RESNA SIG-17 "International Appropriate Technology" Vice-Chair	2009-Present
MIT Graduate Resident Tutor in New House Residence	2005-2010
MIT Hobby Shop Advisory Committee Member	2008-2010
MIT 2.007 "Design and Manufacturing I" contest judge	2004-2008
MIT Graduate Student Council Student Life Grant Review Committee	2007
MIT IDEAS Competition Rowing Wheelchair Advisor	2006
National Society of Black Engineers Program Assistant	2005
St. Paul's School FIRST Robotics Team Volunteer	2005

AMOS G. WINTER, V – RESEARCH STATEMENT

My research group will focus on the creation and scientific investigation of technology for use in highly constrained environments – contexts in which we have limited engineering experience, where physical, social, political, or monetary constraints must be actively addressed during the design process. I will pursue technical challenges relevant to the developed and developing world while engaging in a Global Design process: co-creating technology with stakeholders, characterizing environmental constraints and opportunities, linking environmental parameters to engineering performance, testing designs in context, and pursuing cross-cultural/application technology transfer. My research will be rooted in applications and motivated by scientific understanding, economic advantage, and social impact.

The two principal projects I developed during my PhD - RoboClam and the Leveraged Freedom Chair (LFC) - demonstrate my vision of Global Design research in highly constrained environments. The aim of the RoboClam project was to generate biologically-inspired, low-power, compact, lightweight, and reversible subsea burrowing technology for applications ranging from oil rig anchoring to subsea cable installation [19]. I identified Atlantic razor clams (*Ensis directus*) as prime candidates for biomimicry, quantified their performance in engineering terms, and discovered that they drastically reduce burrowing drag by using motions of their shell to fluidize surrounding soil [17]. Accounting for the soil, solid, and fluid mechanics at play during this event, I derived an analytical model that shows fluidization is created by local soil failure around a contracting clam shell and verified the model through 3D substrate/fluid index of refraction-matched particle image velocimetry in collaboration with Prof. Wolfgang Losert at the University of Maryland [14]. My thesis work culminated in the construction and testing of the RoboClam robot, which used a genetic algorithm to optimize burrowing kinematics in order to achieve the same performance as *Ensis*, with burrowing energy scaling linearly with depth, rather than depth squared for moving through static soil [20, 18, 17].

The LFC is a lever-powered mobility aid designed specifically for use in rural areas of developing countries, where 14 million people need a wheelchair but do not have one [1, 7]. The key innovation behind the device is its single-speed, variable mechanical advantage drivetrain, where the user simply adjusts hand position on the levers to change torque and angular velocity [15]. Human upper body force and power outputs were used to optimize the drivetrain geometry, resulting in a device 10-20% faster on pavement than a wheelchair and more capable off road than any other product available [13]. Since the user changes body geometry to effectively "shift gears," the LFC drivetrain can be made from a simple, single-speed assembly of bicycle components, making the chair manufacturable and repairable anywhere in the world for the same price or less than competing products [16]. My current postdoc activities are focused on quantifying user benefits by comparing biomechanical models to LFC performance and commercializing the chair in India with BMVSS Jaipur Foot, the largest disability organization in the world [4].

In the near term, I will conduct research that leverages skills acquired during my PhD and enables me to branch out into new areas of Global Design. I will investigate the parametric relationships between device size, substrate type, and burrowing performance, both to commercialize RoboClam technology and generate design rules that enable engineers to make RoboClam-inspired devices for any application. Concurrently, I plan to explore extensions of localized fluidization burrowing for dry applications, such as land mine neutralization, bunker reconnaissance, and spacecraft geological surveys. This problem presents further biomimetic opportunities to investigate animals that "swim" through soil, such as the sandfish lizzard (*S. scincus*) [8].

I plan to continue with biomechanics and medical device design for both the developing and developed world. Although much is known about the mechanical performance of human legs [12], there is little understanding of the relationship between upper body kinematics and power output. The anthropomorphic data generated from this research will be applicable to the creation of efficient

mobility aids, as well as general human-centered applications ranging from the design of manually-powered products to assembly line planning. Working with BMVSS Jaipur Foot this year will also provide me with training in prosthetics. With thousands of our troops returning injured from Iraq and Afghanistan, as well as 10 to 25 million amputees in the world [10], there is limitless opportunity for low-cost assistive device innovation and cross-cultural technology transfer.

Other Global Design projects I intend to pursue are unmanned air/sea hybrid systems and smoke-free, ultra low-cost biofuel cookstoves. DARPA is currently funding a program to develop an unmanned vehicle that can operate both underwater and in the air for marine intelligence, surveillance, and reconnaissance (ISR) [3]. I plan to research the governing physical principles that enable flying fish to transition from water to air, varying two orders of magnitude in Reynolds number while using the same control surfaces [5, 6]. Design rules resulting from this research would result in the creation of air/sea vehicles with tremendous value to military and reconnaissance applications. Two and a half billion people are forced to use biomass for cooking fuel and indoor air pollution from cooking kills 1.5 million people annually in the developing world [11]. My research in this area will focus on understanding the combustion, thermodynamics, and heat transfer processes behind existing cookstoves as well as industrial particle ablating incinerator technology. This knowledge, combined with stakeholder input, will be used to design a smoke-free cookstove system that is competitively priced and that can be locally manufactured and distributed through current channels.

In the future, I envision myself becoming a world-recognized leader of Global Design in highly constrained environments. I want to be called on to address challenges ranging from the BP oil spill in the Gulf of Mexico to health technology disseminated by the Gates Foundation. My skill set and career interests position me to become a leader in cross-cultural and inter-market technology transfer, a position from which I want to shepherd a technical and economic resurgence in our country by helping American industry actively engage emerging markets. Commercializing technologies will also be an important facet of my career. I plan to achieve this through industry collaborations, spinning companies out of my lab, and creating a non-profit sister organization to my research group akin to Paul Polak's International Development Enterprises [9]. This concept of an academic/NGO symbiotic relationship has already been successfully implemented by The MIT Abdul Latif Jameel Poverty Action Lab (J-PAL), which is run by development economists from around the world [2]. J-PAL regularly wins multi-million dollar grants from foundations such as Gates and Google to conduct randomized evaluation research of development interventions in partnership with its US-based sister NGO, as well as numerous local stakeholders.

For the past five years, I have chosen activities to hone my skills in preparation for leading an extreme environment Global Design lab. I have successfully managed two large-scale research projects during my PhD, engaging in engineering science throughout the world while cultivating collaborations with top experts and stakeholders in relevant fields. The MIT Mobility Lab, the mobility/disability student research group that I started, partners with 20+ organizations around the world, and I maintain an active relationship with my PhD sponsors Battelle and Bluefin Robotics. During my time at MIT, I raised over $700,000 to support my research activities and I am confident in my abilities to generate funding for the Global Design programs in my lab. Towards this end, I worked with ASME to develop the curriculum for an NSF workshop on design for extreme affordability research, which will be held this spring. Additionally, I am exploring Indian-focused technology research projects that could be implemented globally with Battelle's India office.

My work has gained recognition from CNN, the Discovery Channel, the Wall Street Journal, and Scientific American, has been featured on the front page of the Boston Globe, and has received accolades including first place in ASME's Innovation Showcase and an R&D 100 award. After advising 20 students through MIT's Undergraduate Research Opportunities Program and seven undergraduate theses, I am confident in my abilities to lead a lab, attract excellent students, and guide them in conducting novel research while developing their own intellectual growth.

References

[1] *Annual Program Statement*. United States Agency for International Development, 2003.

[2] The Abdul Latif Jameel Poverty Action Lab. `http://www.povertyactionlab.org/`, 2010.

[3] Bluefin Robotics and Aurora Flight Sciences. Pelican project. personal conversations, October 2010.

[4] BMVSS Jaipur Foot. What is our Progress? `http://www.jaipurfoot.org/02_progress_performance.asp`, 2007.

[5] J. Davenport. Allometric constraints on stability and maximum size in flying fishes: implications for their evolution. *Journal of Fish Biology*, 62(2):455–463, 2003.

[6] F.E. Fish. Wing design and scaling of flying fish with regard to flight performance. *Journal of Zoology*, 221(3):391–403, 1990.

[7] N.E. Groce. Health beliefs and behavior towards individuals with disability cross-culturally. *Cross-cultural rehabilitation, An international perspective*, pages 37–47, 1999.

[8] R.D. Maladen, Y. Ding, C. Li, and D.I. Goldman. Undulatory swimming in sand: Subsurface locomotion of the sandfish lizard. *Science*, 325(5938):314, 2009.

[9] P. Polak. *Out of poverty: what works when traditional approaches fail*. Berrett-Koehler Publishers, 2008.

[10] C.K. Prahalad. *The fortune at the bottom of the pyramid: Eradicating poverty through profits*. Wharton, 2010.

[11] K. Watkins et al. *Human Development Report 2007/2008: Fighting climate change: Human solidarity in a divided world*. United Nations Development Programme, 2007.

[12] D.G. Wilson, J. Papadopoulos, and F.R. Whitt. *Bicycling science*. The MIT Press, 2004.

[13] A.G. Winter, M.A. Bollini, D.H. DeLatte, H.F. O'Hanley, and N.K. Scolnik. The design and testing of a low-cost, globally-manufacturable, multi-speed mobility aid designed for use on varied terrain in developing and developed countries. In *Proceedings of the ASME 2009 International Design Engineering Technical Conferences and Computers and Information in Engineering Conference*, number DETC2009-87609, 2009.

[14] A.G. Winter, V. *Biologically Inspired Mechanisms for Burrowing in Undersea Substrates*. PhD Thesis in Mechanical Engineering, Massachusetts Institute of Technology, 77 Massachusetts Ave., Cambridge, MA 02139, Sept. 2010.

[15] A.G. Winter, V, M.A. Bollini, X. Chen, D.H. DeLatte, D.D. Frey, B.H. Gallup, D. Hicks, G.M. Jones, B. Judge, H.F. O'Hanley, N. Ruleman, and N.K. Scolnik. Wheelchair with Lever Drivetrain. US patent application no. 12914986, October 2010.

[16] A.G. Winter, V, M.A. Bollini, D.H. DeLatte, H.F. O'Hanley, Pearlman J.L., and N.K. Scolnik. The design, fabrication, and performance of the east african trial leveraged freedom chair. In *Proceedings of the ASME 2010 International Design Engineering Technical Conferences and Computers and Information in Engineering Conference*, number DETC2010-29096, 2010.

[17] A.G. Winter, V, R.L.H. Deits, D.S. Dorsch, Slocum A.H., and A.E. Hosoi. Razor Clam to RoboClam: Burrowing Drag Reduction Mechanisms and their Robotic Adaptation. *In preparation, to be submitted to the Proceedings of the National Academy of Sciences*, 2011.

[18] A.G. Winter, V, R.L.H. Deits, D.S. Dorsch, A.E. Hosoi, and A.H. Slocum. Teaching RoboClam to Dig: The Design, Testing, and Genetic Algorithm Optimization of a Biomimetic Robot. In *Proceedings of the IEEE/RSJ 2010 International Conference on Intelligent Robots and Systems (IROS)*, number WeET11.3, 2010.

[19] A.G. Winter, V, A.E. Hosoi, and A.H. Slocum. Method and Apparatus for Penetrating Particulate Substrates. US patent application no. 12455392, June 2009.

[20] A.G. Winter, V, A.E. Hosoi, A.H. Slocum, and R.L.H. Deits. The design and testing of roboclam: A machine used to investigate and optimize razor clam-inspired burrowing mechanisms for engineering applications. In *Proceedings of the ASME 2009 International Design Engineering Technical Conferences and Computers and Information in Engineering Conference*, number DETC2009-86808, 2009.

AMOS G. WINTER, V – TEACHING STATEMENT

Our call as educators is to prepare the next generation of engineers to tackle the most pressing scientific and technological challenges facing the world. These students will need to integrate into a global marketplace that is markedly different from the developed world-focused industry that has largely persisted since World War II. China and India are projected to have the first and third largest economies, respectively, by 2050 [6], and combined with Brazil and Russia, are forecasted to grow from 18% global market capital now to 41% in 2030 [5]. We are on the cusp of a new industrial revolution in emerging markets, with one billion+ new consumers who will demand products to meet their specific needs, and another billion+ who will make less than a dollar per day but require innovative technologies to rise out of poverty [7]. I want to be a leader in training students as Global Engineers who are capable of addressing technical problems anywhere in the world and who can catalyze a resurgence in US industry by helping it engage rapidly developing economies. My classes will combine rigorous engineering theory with practical applications and understanding of factors that affect commercialization, including economics, cultural differences, and usage practices. I will inspire students to become engineers by elucidating how their technical skills can be used to make a positive impact on the world.

Much of my desire to become a professor comes from a love of teaching and mentoring. For the past four years, I have taught SP.784 Wheelchair Design in Developing Countries (WDDC) [8] at MIT. Through WDDC, students collaborated with wheelchair builders and disability organizations throughout the world to create technology and business opportunities for people with disabilities in developing countries. Designing this class required developing hands-on exercises, role-plays, and readings that engaged students from virtually every major, building collaborations with 20+ international partners and inviting many to visit MIT for guest lectures, and creating opportunities with the MIT Public Service Center and Undergraduate Research Opportunity Program (UROP) for students to travel abroad and implement projects with local partners. The desire of students to pursue long-term, large-scale mobility projects inspired me to create the MIT Mobility Lab (M-Lab) [2], which is now an integral part of MIT's international development D-Lab program [1]. M-Lab gives students a physical workspace and an organization within which to develop and disseminate novel mobility-focused research.

To date, 80+ students have participated in M-Lab programs, with more than 20 traveling abroad to implement projects. Seventy percent of WDDC students and sixty percent of M-Lab UROP/thesis students have been women. Students under my direct supervision have won Rhodes, Truman, Hertz, and National Defense Science and Engineering Graduate Fellowships. In the spring of 2010, I was awarded the MIT School of Engineering Graduate Student Extraordinary Teaching and Mentoring Award, the highest honor given to a graduate student for teaching and mentoring at the Institute. I have consummately demonstrated my abilities as an educator during my time at MIT, both through the success of my programs and the recognition of the students I have inspired.

I am a firm believer in hands-on learning. Everyone has a baseline understanding of engineering principles by simply being a participant in the physical world. As a teacher, I like to leverage this by adding theory to intuition, or building intuition upon theory for those students more mathematically inclined. Using hands-on examples engages <u>all</u> students in the classroom and facilitates mental connections between theory and application, no matter to which side a student is predisposed. For example, in my elastic beam bending lecture in WDDC I gave each student geometrically identical beams of polycarbonate, 6061-T6 aluminum, and 6061-T0 aluminum so they could feel differences in bending stiffness, bending strength, and moment of inertia while I derived corresponding theory.

Whenever possible, I will invite industry professionals and fellow academics to visit my classes to discuss lecture theory in practice. In WDDC, guest lectures given by developing world wheelchair users and manufacturers always made a profound impression; they put a real "face" on the challenges we were addressing. Transcending textbook problems, teaching engineering in action, and

showing students first-hand how they can positively impact society through technology is a tremendous motivator, which often attracts students from demographics that are underrepresented in engineering. This is demonstrated by >50% female enrollment in MIT D-Lab program classes, which annually have more than 200 students [3].

I plan to develop a new graduate course on Global Design. At its root, the class will be composed of a rigorous curriculum including mechanical design, precision machine design, and product design. Beyond engineering fundamentals, this class will train students to solve critical technical problems within a global context. They will learn about geographically-dependent user preferences, economic issues that affect commercialization, commercial and donation-based strategies for international development – factors just as important as nuts, bolts, and number crunching in determining the success of a technology. For example, I will include a case study on the Tata Nano – a car of bare-bone simplicity, but one that required revolutionary production techniques to hit a sale price of $2,000, within reach of the Indian consumer who typically could only afford a motorcycle [4].

Student teams in Global Design will pursue term-long projects to develop a new technology from inception to proof-of-concept prototype. Projects will range from: ultra low-cost, poverty alleviating technologies for developing countries, such as point-of-use, minimum drainage and evaporation irrigation systems; mid-range, consumer-focused products for emerging markets, such as portable x-ray machines for rural health workers; and high-tech commercial devices, such as anchoring systems for offshore wind farms. Each team will work in collaboration with stakeholders from around the world composed of industry professionals, implementers of technology (such as doctors or non-governmental organizations), and end users. Part of the collaborative element of the class will be guest lecturers given by stakeholders and other experts in fields related to course material. I will use this class as an incubator for research projects and a means of identifying stellar students for my lab.

In addition, there are a number of core undergraduate classes that I would love to teach and enhance with new modules. As part of the machine design curriculum, I would like to develop an"Engineering in Action" portion of each lecture, which would present a real-life engineering problem that directly correlates to theory covered in class. This would not be just a chalkboard or powerpoint example; Engineering in Action would include guest lectures by industry professionals, short movies showing technology in the field, and live demos of machines. Each presentation would end with the posing of a problem that the students would solve as homework, such as calculating loads in a crane, figuring out the wall thickness of a pressure vessel, or scaling the size of an electric motor. The problems would intentionally be open-ended to force the students to work like real engineers, seeking additional information. In the same vein as a PhD qualifying oral exam, the students would present their solutions during lab section.

I would like to develop a section on soil mechanics as part of the solid mechanics curriculum. For many engineers, soils are an unfamiliar and strange material; the concepts of depth-dependent yield strength and velocity-independent shear stress do not fit within the understanding of solid and fluid constitutive behavior most of us develop as undergraduates. This section would instill an elementary grasp of soil behavior, as many engineering systems, such as anchors, oil wells, and construction equipment, interact with soils.

In all of the avenues presented in this statement, I will combine my passion for teaching, connections between engineering theory and application, and a worldwide view of technological innovation and dissemination to inspire students to become Global Engineers.

References

[1] MIT D-Lab Program. http://d-lab.mit.edu/, 2010.

[2] MIT Mobility Lab. http://mlab.mit.edu/, 2010.

[3] Personal conversations with Victor Grau Serrat, co-director of the MIT D-Lab program, May 2010.

[4] R.A. Mashelkar. Breakthrough designs for ultra-low-cost products. http://www.ted.com/talks/r_a_mashelkar_breakthrough_designs_for_ultra_low_cost_products.html, November 2009.

[5] T. Moe, C. Maasry, and R. Tang. Global Economics Paper No. 204, EM Equity in Two Decades: A Changing Landscape. Technical report, Goldman Sachs, 2010.

[6] J. O'Neill. *BRICs and Beyond*. Goldman Sachs Global Economics Group, 2007.

[7] P. Polak. *Out of poverty: what works when traditional approaches fail*. Berrett-Koehler Publishers, 2008.

[8] A.G. Winter, V. MIT Class SP.784 Wheelchair Design in Developing Countries. http://web.mit.edu/sp.784/www/index.html, 2010.

Razor Clam to RoboClam: Burrowing Drag Reduction Mechanisms and their Robotic Adaptation

Amos G. Winter, V,[1*] Robin L. H. Deits,[1] Daniel S. Dorsch,[1]
Alexander H. Slocum[1], A. E. Hosoi,[1]

[1]Department of Mechanical Engineering, Massachusetts Institute of Technology
77 Massachusetts Ave., Cambridge, MA 02139, USA

[*]To whom correspondence should be addressed; E-mail: awinter@mit.edu.

Submitted to *Science*, Dec. 2010

Estimates based on the strength, size, and shape of *Ensis directus*, a burrowing bivalve commonly known as the Atlantic razor clam, indicate that its burrow depth should be physically limited to a few centimeters; yet the organism can dig as deep as 70cm. By measuring soil deformations around burrowing *Ensis*, we have discovered that these animals reduce drag by using motions of their valves to locally fluidize the surrounding substrate. As *Ensis* initiates its digging cycle, it creates a soil failure surface 1–4 body radii away from the contracting valves. Further contraction draws water towards the animal, which mixes with the failed soil to create a fluidized pocket. The energy associated with motion through this fluidized medium – characterized by a depth-independent density and viscosity – scales linearly with depth. In contrast, moving through static soil requires energy that scales with depth squared. For *Ensis*, this translates to a 10X reduction in the energy required to

reach observed burrow depths. The extent of the fluidized zone is dictated by two commonly-measured geotechnical parameters: coefficient of lateral earth pressure and friction angle. Calculations using typical ranges for both parameters indicate that this digging strategy should be effective in any particulate soil type, regardless of cohesion, particle size, and depth. For engineers, localized fluidization offers a method to dramatically reduce burrowing energy with a mechanically simple, self-contained burrowing device. We demonstrate this concept with RoboClam, a robotic prototype of such a system, in which we have used a genetic algorithm to find optimal digging kinematics to achieve burrowing performances comparable to those of the live organism in widely different soil types: idealized granular glass beads and *Ensis'* native cohesive mudflat habitat.

Burrowing in soil presents challenges in engineering and biological applications alike. Many animals have developed unique locomotion schemes to move through particulate substrates (*1*). The sandfish lizard (*S. scincus*) undulates in the manner of a fish in order to effectively swim through sand (*2*). Clam worms (*N. virens*) have been observed to use crack propagation to burrow in gelatin, a material with similar properties to elastic muds (*3*). Smaller organisms, like *C. elegans*, have been observed to move efficiently via reciprocating motion in saturated granular media (*4, 5*). Contrary to a generalized Newtonian fluid, in which viscosity and density do not change with depth, particles within a granular material experience contact stresses, and thus frictional forces, that scale with the surrounding pressure, resulting in shear strength that increases linearly with depth (*6*). This means that submerging devices such as anchors and piles can be costly, as insertion forces $F(z)$, increase linearly with depth z (*7*), resulting in an insertion energy, $E = \int F(z)\, dz$, that scales with depth squared. *Ensis directus*, the Atlantic razor clam, can produce approximately 10N of force to pull its valves into soil (*8*). Using

measurements from a blunt body the size and shape of *Ensis*, we determined that this level of force enables the clam to submerge to approximately 1–2cm into a packed bed. But in reality, *Ensis* digs to 70cm (*9*), indicating that the animal must manipulate surrounding soil to reduce burrowing drag and the energy required for submersion.

Ensis burrows by using a series of valve and foot motions to draw itself into the substrate, as shown in Figs. 1A–F. An upper bound of the mechanical energy associated with digging can be estimated by adapting results from Trueman (*8*) and summing the energies and kinematics associated with each stage during one burrow cycle: valve uplift (0.05J, -0.5cm), valve contraction (0.07J, 0cm), and valve penetration (0.20J, 2.0cm), combine for a total of 0.21J/cm. Re-expansion of the valves is accomplished through elastic rebound of the hinge ligament, and thus requires no additional energy input by the animal. Comparing this performance, in Fig. 1G, to the energy required to push an *Ensis*-shaped blunt body into the animal's habitat substrate using steady downward force, we find the animal is able to reduce its required burrowing energy by an order of magnitude, even though there is an energetic cost associated with pushing up and contracting its valves – motions that do not directly contribute to downward progress.

To investigate the soil mechanics at play during *Ensis* burrowing, we constructed a visualization system to see through the substrate surrounding a burrowing animal and measure deformation of the granular medium with particle image velocimetry (PIV) (*10*). A full description of our experimental setup is included in the supporting online material for this paper. Our testing revealed that *Ensis* uses the uplift and contraction movements of its valves to create a fluidized pocket around its body, as shown by the PIV results in Figs. 2B and C.

The lower region of the fluidized soil pocket is created during the valve uplift stroke of *Ensis'* burrowing motions. In the substrate used in our laboratory experiments – seawater-saturated 1mm soda lime glass beads, which are nearly the same size and density as coarse sand (*6*) – the water flow velocity required to induce fluidization is calculated to be approximately

1.35cm/s (*11–14*). The valve uplift velocity in the trial associated with the results in Fig. 2 was measured to be 1.05 ± 0.05cm/s. The valve uplift velocity reported by Trueman was 1.25cm/s (*8*), indicating that the uplift velocity of live *Ensis* is on the order of the required fluidization velocity. Note that 1.35cm/s is an upper bound for required fluidization velocity, as naturally occurring substrate particles in *Ensis* habitats are typically smaller than 1mm, and hence require lower fluidization velocities (*9*).

Fluidization on the sides of *Ensis* during valve contraction occurs via localized failure in the soil. At the initiation of valve contraction, the horizontal stress acting between the valves and the soil is reduced to a point where the imbalance between horizontal and vertical stresses creates a resolved shear stress that exceeds the shear strength of the soil (*6*). The angle of the failure surface in plane strain, which is the kinematic condition of our 2D PIV experimental setup, can be predicted as $\theta_f = 45^\circ + \frac{\phi}{2}$, where ϕ is the friction angle, an independently measured soil property. This relationship can be derived geometrically from the Mohr's circle (*15*) stress representation in Fig. S3A in the supporting online material. The friction angle in our 1mm soda lime glass beads was measured as 24.7°, yielding a failure angle of 57.4°, which is shown with the dotted line superimposed on the PIV image in Fig. 2D. Note that Figs. 2C and D occur at different times; *Ensis* valve movements are associated with a timescale much shorter than the time required for natural soil collapse around the clam. This explains why the full failure wedge can only be seen after valve contraction, when the soil in the failure zone has sufficient time to unpack and slide towards the burrowing organism (*6, 16*).

The discontinuity at the failure surface enables fluidization to occur; as the valves contract beyond the point of incipient failure, the particles in the failure zone are free to move with the pore fluid while the particles outside the failure zone remain stationary. The relevant Reynolds number of the pore fluid flow, $\mathrm{Re} = \frac{\rho_f V d_p}{\mu_f}$, calculated from *Ensis'* valve velocity V, particle diameter d_p, and the pore fluid density ρ_f and viscosity μ_f, varies between 0.02 and 56, depending

on particle size (0.002 to 2mm (*6, 8, 9*)), animal size (10 to 20cm (from experimental observation)), and valve contraction velocity (v $\approx$ 0.011 to 0.028m/s (*8*)). As this range of Reynolds numbers falls primarily within the regime of Stokes drag (the transition to form drag occurs at a Reynolds number of approximately 100), the characteristic time for a 1mm soda lime glass bead to reach the pore fluid velocity can be estimated through conservation of momentum (*17*): $\tau = \frac{{d_p}^2 \rho_p}{36\mu_f} = 0.075s$ where ρ_p is the density of the bead. This timescale is considerably less than the $\approx$ 0.2s valve contraction time measured by Trueman (*8*), indicating that soil particles surrounding *Ensis* can be considered inertialess and are advected with the pore fluid during valve contraction.

The discontinuity created by the failure surface is critical to achieving fluidization, as without it substrate particles would follow the fluid flow field, which is incompressible and governed by $\nabla \cdot \overline{v} = 0$. No divergence in the flow field creates no divergence between particles, and thus no unpacking. However, in the presence of a finite failure zone, *Ensis'* contraction motion reduces the volume of the organism, which draws pore water into the region surrounding the animal. This pore water mixes with the failed soil to create a *locally* unpacked, fluidized zone. Figure 2C shows the fluidized zone surrounding *Ensis* during its contraction motion. The PIV results are plotted as the current void fraction ϵ divided by the initial void fraction ϵ_i. Areas where $\frac{\epsilon}{\epsilon_i} > 1.05$ show regions of fluidization, as the particles have separated beyond the void fraction at incipient fluidization, $\epsilon = 0.41$ (*11*).

A fluidized substrate can, to first order, be modeled as a generalized Newtonian fluid with a density and viscosity that are functions of the local packing fraction (*18–23*). This implies that *Ensis* could achieve depth-independent drag resistance and hence a digging energy that scales linearly with depth, as the parameters of a generalized Newtonian fluid do not depend on hydrostatic pressure. This hypothesis is supported by the results of Trueman (*8*), in that *Ensis* burrowing kinematics change little with depth, and is demonstrated in Fig. 1G by the

linear relationship between energy and displacement. Contrast this with the blunt body pushed through static soil, also shown in Fig. 1G, where, as expected, penetration energy scales with depth squared.

To verify that localized fluidization drag reduction can be transferred to engineering applications, we built RoboClam, the robot shown in Fig. 3. RoboClam replicates *Ensis* digging kinematics and lends insight into the relationships between environmental and engineering burrowing parameters, such as substrate type, depth, device size, velocity, and required power. The robot consists of a control platform with two pneumatic pistons that actuate the two degrees of freedom of an *Ensis*-like end effector. Pneumatics were chosen as the main power source so RoboClam can be safely tested in real, undisturbed ocean substrates without container wall effects. Burrowing kinematics are optimized with a genetic algorithm (GA) (*24*) that approximates the evolution of a biological system by generating a population of parameters, in our case the up/in/down/out displacements, times, and pressures, and then selecting the sets of parameters that yield the minimum 'cost', related to burrowing efficiency.

Figure 4A shows data from the best digging trial obtained during 125 tests in real *Ensis* habitat off the coast of Gloucester, MA. During these tests, the GA varied up and down time, in and out displacement, and the pressures associated with each movement. The optimized cost was the product of the energy expended per unit depth and the exponent of the energy versus depth power law relationship. The product of these parameters was used to evaluate cost because optimizing either individually often led to undesirable values of the other. As can be seen from the figure, RoboClam achieved nearly depth-independent drag resistance, with an energy versus depth power law slope of $n = 1.17$. To contrast this, data from pushing an *Ensis*-shaped blunt body into the same substrate is included in the plot, yielding an expected higher power law relationship with a best-fit of $n \approx 2$.

Figure 4B shows the best digging trial obtained during RoboClam lab testing in 1mm soda

lime glass beads. Through hundreds of tests performed over a period of months, it was determined, through both GA results and observation of the machine, that burrowing performance is most sensitive to in and out motions of the end effector. The test shown in 4B involved no active up and down movements, with the robot propelled merely by its own weight. Digging data in this plot demonstrates a perfectly linear relationship between burrowing energy versus depth, indicating depth-independent drag resistance. The pushing data shown, which exhibits the expected power law relationship of $n \approx 2$, was obtained by pushing the robot into the substrate with steadily increasing force, as shown in inset b.

Surprisingly, the data in Fig. 4 show that the RoboClam can burrow with localized fluidization in two substrates with vastly different properties: one ideally granular (Fig. 4B) and the other inhomogeneous, cohesive, and with organic content (Fig. 4A). This can be rationalized by calculating the soil failure zone around the end effector when it contracts its valves. Combining the stress distribution in the soil around an axially symmetric end effector, described by thick-walled pressure vessel equations (*25*), with the soil stress state at failure yields an expression for a cylindrical failure surface. Under the simplifying assumption that the end effector in Fig. 3 completely removes pressure against the soil during contraction, this expression indicates that the failure radius scales as $\frac{R_f}{R_0} \approx (K_a - K_0)^{-1/2}$, where R_f is the failure radius and R_0 is the end effector radius. A full derivation of this relationship is included in the supporting online material. The coefficient of active failure, $K_a = \frac{1-\sin\phi}{1+\sin\phi}$, is the ratio of horizontal to vertical effective stress at failure and can be derived geometrically from the Mohr's circle in Fig. S3A. The coefficient of lateral earth pressure, K_0, is the ratio of undisturbed horizontal to vertical effective stress. Values for K_0 and ϕ are typically measured during a geotechnical survey (*26*). For real soils, where K_0 ranges from 0.31 to 1 and K_a from 0.19 to 0.52 under most conditions (*6, 27*), the failure zone around a razor clam or RoboClam's end effector will vary from $1 < \frac{R_f}{R_0} < 4$. This means soil failure is a localized effect and that fluidization will

occur whenever the effector, or *Ensis*, contracts and pulls water into the failure zone.

The data and analysis presented in this paper indicate that localized fluidization burrowing should be possible in nearly any type of soil, regardless of cohesion and particle size. The ability to achieve depth-independent drag resistance in a wide variety of substrates is tremendously valuable and may find application in the military, oil, mining, anchoring, oceanographic, and underwater cable industries.

References and Notes

1. E. Trueman, *The locomotion of soft-bodied animals* (Elsevier Science & Technology, 1975).

2. R. Maladen, Y. Ding, C. Li, D. Goldman, *Science* **325**, 314 (2009).

3. K. Dorgan, P. Jumars, B. Johnson, B. Boudreau, E. Landis, *Nature* **433**, 475 (2005).

4. H. Wallace, *Annual Review of Phytopathology* **6**, 91 (1968).

5. S. Jung, *Physics of Fluids* **22**, 031903 (2010).

6. K. Terzaghi, R. Peck, G. Mesri, *Soil mechanics in engineering practice* (Wiley-Interscience, 1996).

7. P. Robertson, R. Campanella, *Canadian Geotechnical Journal* **20**, 718 (1983).

8. E. Trueman, *Proceedings of the Royal Society of London. Series B. Biological Sciences* **166**, 459 (1967).

9. A. Holland, J. Dean, *Chesapeake Science* **18**, 58 (1977).

10. J. Sveen, An introduction to MatPIV v. 1.6.1, `http://folk.uio.no/jks/matpiv/` (2004).

11. C. Wen, Y. Yu, *Chem. Eng. Prog. Symp. Ser* (1966), vol. 62, pp. 100–111.

12. J. Richardson, W. Zaki, *Chemical Engineering Research and Design* **32**, 35 (1954).

13. A. Khan, J. Richardson, *Chemical Engineering Communications* **78**, 111 (1989).

14. L. Gibilaro, *Fluidization-dynamics* (Butterworth-Heinemann Oxford, UK, 2001).

15. R. Hibbeler, *Mechanics of Materials* (Prentice Hall, 2000), fourth edn.

16. D. Wood, *Soil behaviour and critical state soil mechanics* (Cambridge Univ Pr, 1990).

17. P. Kundu, I. Cohen, *Fluid Mechanics* (Elsevier Academic Press, 2004).

18. A. Einstein, *Annalen der Physik* **19**, 289 (1906).

19. N. Frankel, A. Acrivos, *Chemical Engineering Science* **22**, 847 (1967).

20. I. Krieger, T. Dougherty, *Journal of Rheology* **3**, 137 (1959).

21. H. Eilers, *Kolloid, Z.* **97**, 313 (1941).

22. F. Ferrini, *et al.*, *Rheologica Acta* **18**, 289 (1979).

23. S. Maron, P. Pierce, *Journal of colloid science* **11**, 80 (1956).

24. R. Haupt, S. Haupt, *Practical genetic algorithms* (Wiley-Interscience, 2004).

25. S. Timoshenko, J. Goodier, *Theory of elasticity* (McGraw, New York, 1970).

26. ASTM Standard D4767, DOI: 10.1520/D4767-04, Standard Test Method for Consolidated Undrained Triaxial Compression Test for Cohesive Soils, `http://www.astm.org/Standards/D4767.htm` (ASTM International, 2003).

27. T. Lambe, R. Whitman, *Soil mechanics* (John Wiley & Sons Inc, 1969).

28. E. Avallone, T. Baumeister, A. Sadegh, *Marks' standard handbook for mechanical engineers* (McGraw-Hill New York etc., 1987).

29. A. Slocum, *Precision machine design* (Society of Manufacturing, 1992).

30. This work was supported by the Battelle Memorial Institute, Bluefin Robotics, and the Chevron Corporation. We thank M. Bollini, C. Jones, and D. Sargent for experimental assistance.

Figure captions

Figure 1: *Ensis* digging cycle kinematics and energetics. Dotted line in A)-F) denotes a depth datum. White arrows indicate valve movements. Red silhouette denotes valve geometry in expanded state, before contraction. A) *Ensis* at initiation of digging cycle. B) Extension of foot. C) Valve uplift. D) Valve contraction, which pushes blood into the foot, expanding it to serve as a terminal anchor. E) Retraction of foot and downwards pull on the valves. F) Valve expansion, reset for next digging cycle. G) Energetic comparison showing that *Ensis* requires an order of magnitude less energy to submerge to burrow depth than a blunt body of the same size and shape pushed into static soil. As predicted, because *Ensis* moves through locally fluidized soil, its burrowing energy scales linearly with depth, rather than depth squared. *Ensis* data adapted from (*8*). Blunt body data collected from 15 penetration tests in real *Ensis* habitat off the coast of Gloucester, MA

Figure 2: Temporal evolution of fluidized zone around burrowing *Ensis*. PIV data overlaid on original video frames. Data plotted as current void fraction ϵ divided by initial void fraction ϵ_i. Colored areas show regions of localized fluidization. Timeline on left side of figure shows progression of burrowing events. A) Initiation of burrowing cycle. B) Completion of valve uplift, corresponding to Fig. 1C. C) Completion of valve contraction, corresponding to Fig. 1D. D) Moment when failure wedge fully forms, occurring after retraction of foot and downwards pull on valves, corresponding to Fig. 1E. The failure wedge develops on a longer timescale than fluidization by valve uplift and contraction, which is clearly seen by the timeline. Predicted failure wedge angle, θ_f, calculated from the substrate friction angle and shown with the dotted line, matches well with the PIV data wedge angle seen in D).

Figure 3: Anatomy of the RoboClam. A) RoboClam burrowing in *Ensis* habitat on a mudflat in Gloucester, MA. Labels correspond to the robot's actuators: in-out piston (IOP); and up-down piston (UDP). B) Close-up of the end effector (within dashed line box) in relation to the robot. Picture taken at beginning of burrowing, before penetration of the soil. C) Sectioned view of end effector mechanism. Labels: inner rod (IR); outer rod (OR); top nut (TN); side shell (SS); neoprene boot (NB); wedge (W); and leading tip (LT). End effector moved up and down by motion of the top nut, which is connected to the up-down piston through the outer rod. Opening and closing of the end effector accomplished by sliding the wedge, which is connected to the in-out piston through the inner rod, within the side shells. The neoprene boot protects the mechanism from jamming with soil. The leading tip protects the neoprene boot from tearing. D) Exploded view of end effector showing contact points, which exactly constrain the mechanism, providing deterministic loading and jam-free operation.

Figure 4: RoboClam burrowing data showing energetic advantages of localized fluidization. A) Total burrowing energy versus depth data from best test, determined by genetic algorithm, out of 125 tests gathered in *Ensis* habitat in Gloucester, MA. Pushing data from *Ensis*-shaped blunt body in same location. Power law exponent of digging near ideal of $n = 1$ due to localized fluidization; pushing data near expected value of $n = 2$ for moving in static soil. Inset a) shows burrowing commands given to the robot, plotted as piston pressure and movement times. Inset b) shows increase in required downward pushing force with depth in static soil, but relatively constant force in fluidized substrate. B) Total burrowing energy versus depth data from best test, determined from ideal $n = 1$, out of 54 performed in 1mm soda lime glass beads. Pushing data from robot slowly submerging into substrate under increasing down pressure. Contrast between methods shows depth-independent drag and energy savings achieved by digging rather than pushing. Only in and out motions of the end effector were actively controlled during digging

tests, shown by inset a), with the robot allowed to fall under gravity, shown by inset b). A) and B) demonstrate that localized fluidization burrowing is viable in a wide variety of soil types, ranging from ideally granular to cohesive.

Figures

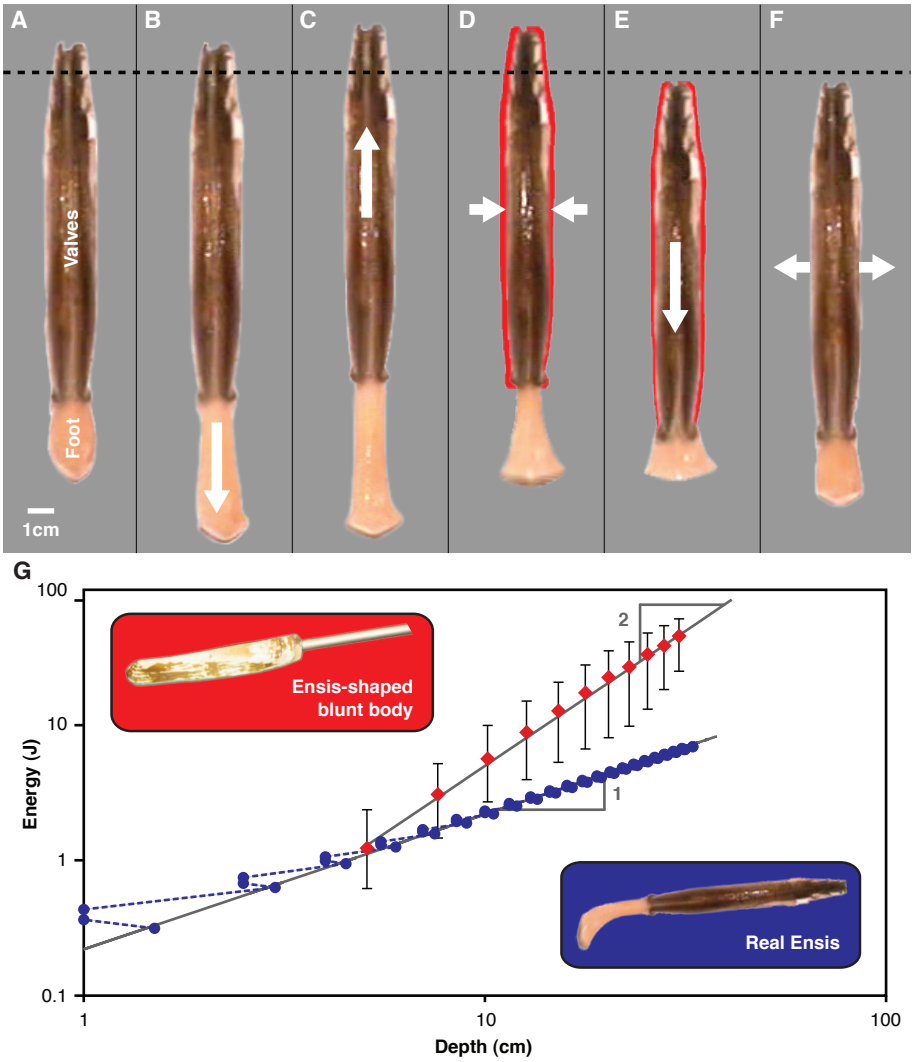

Figure 1: *Ensis* digging cycle kinematics and energetics (figure enlarged for review; actual width = 12cm - double column).

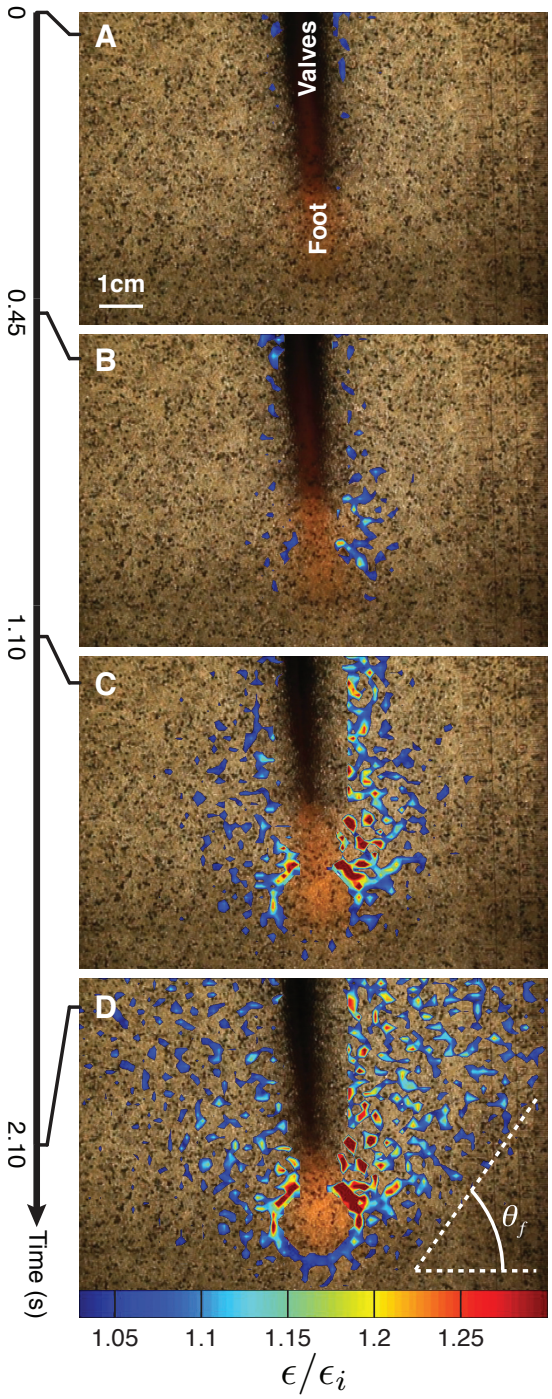

Figure 2: Temporal evolution of fluidized zone around burrowing *Ensis* (figure enlarged for review; actual width = 5.5cm - single column).

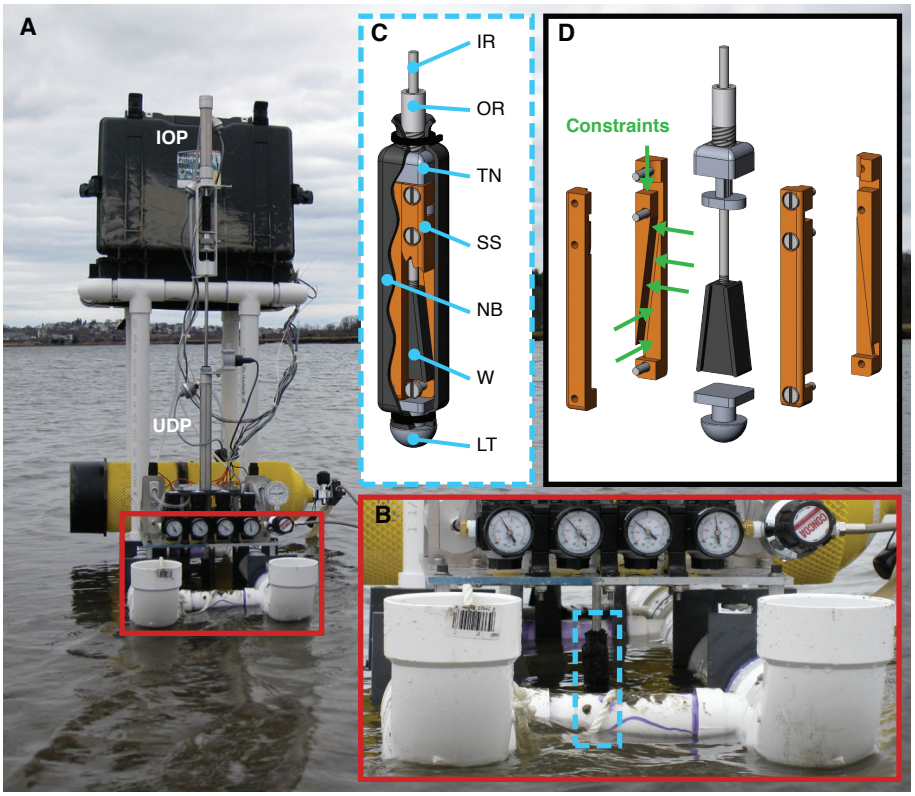

Figure 3: Anatomy of the RoboClam (figure enlarged for review; actual width = 12cm - double column).

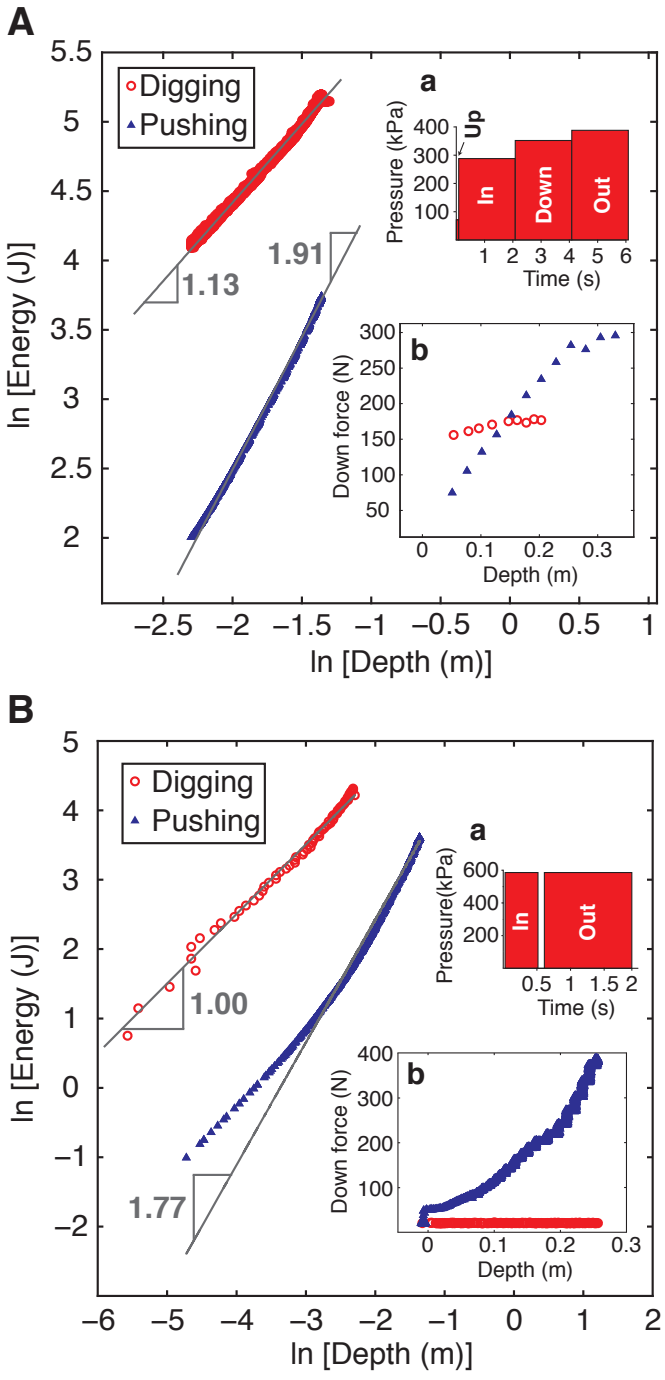

Figure 4: RoboClam burrowing data showing energetic advantages of localized fluidization (figure enlarged for review; actual width = 5.5cm - single column).

Supporting online material

Burrowing visualization system

Ensis specimens used in this research were collected in Gloucester and Orleans, Massachusetts. Burrowing motions, as well as deformations in the soil surrounding the animal, were visualized using the apparatus in Fig. S1A. The tank is essentially a Hele-Shaw cell, commonly used in fluid mechanics experiments to measure flow in two dimensions (*17*). The front viewing pane is adjustable forward and aft via lead screws and bellowed side walls, allowing tank and animal thickness to be matched. Specimens in the tank are visualized in silhouette by three halogen lamps mounted behind the substrate, as shown in Fig. S1B.

The substrate used in the visualizer is 1mm diameter, optically clear soda lime glass beads. This substrate was chosen because its density of 2.52 g/cm^3 is close to that of silica sand, 2.63 g/cm^3 (*6*), one of the substrates in which *Ensis* lives (*9*). Through experimentation, we found that light transmission through the substrate increased with particle size. One-millimeter beads were determined as the best experimental substrate because they fall within the size scale of coarse sand grains (*6*) and provide adequate visualization of test animals.

Figure S1C shows the fluid circuit diagram of the heat dissipation and recirculation system in the visualizer. Chilled and oxygenated water is supplied from a commercial lobster tank used to hold specimens. This water is mixed with hot water flowing out of the visualizer and gravity-fed into a pump. The pump sends water to a reservoir with a float valve that maintains fill level near the top of the visualizer. Two outlets leave the reservoir: one into the top of the visualizer, and one directly back to the lobster tank. Because the flow resistance through the substrate within the visualizer is much greater than the resistance of the "short circuit" line from the reservoir to the lobster tank, the portion of heated water that enters the supply stream at the pump is small compared to chilled water from the lobster tank. As a result, we are able

to maintain temperature in the visualizer to within 2°C of the lobster tank, which is set to 10°C.

Opaque particles are interspersed and tracked using Particle Image Velocimetry (PIV) (*10*) to measure deformations and fluidization. A concentration of 7% opaque particles was found to give the best PIV resolution, with an error of $\pm 4\%$.

RoboClam design

A requirement of RoboClam was that it could be tested in real marine substrates, as to avoid wall effects caused by a container, and to capture the peculiarities of real soil with heterogeneous composition and the presence of organic matter. For saltwater compatibility, RoboClam's main power source is an 80 ft^3 scuba tank. Small lead acid batteries power four solenoid valves and digital pressure regulators that direct air to two pneumatic pistons, which control the end effector's two degrees of freedom. Distances are measured by potentiometers attached to each piston.

The end effector's in/out motion is accomplished with a sliding wedge between the two "shells," as shown in Fig. S2A. The parts are made from alloy 932 (SAE 660) bearing bronze and 440C stainless steel. These materials were chosen because both are saltwater compatible and have a low dynamic coefficient of sliding friction when lubricated (*28*), which was measured to be 0.173 with a standard deviation of 0.013. Silicon oil was used as a lubricant because it is not absorbed by the neoprene boot. This mechanism is exactly constrained and has contact lengths/widths greater than two to prohibit jamming during any part of the stroke (*29*). Furthermore, the wedge intersects the center of pressure on the shell regardless of its position. This prevents the shell from exerting moments on the wedge that could increase frictional losses. Fig. S2B shows the free body diagram of end effector components, from which the mechanism efficiency can be calculated as

$$\eta = \left(\frac{\cos\theta - \mu \sin\theta}{\sin\theta + \mu \cos\theta} - \mu \right) \sin\theta \tag{S1}$$

where θ is the wedge angle and μ is the coefficient of friction between sliding parts. From Eq. S1, the energetic sinks in the machine can be accounted for and energy lost to soil deformation during burrowing is deterministically measured.

A laptop controls the robot using a genetic algorithm (GA). This method of control was chosen because GAs facilitate the exploration of a large parameter space and may locate global minima, in situations in which other optimization methods do not (*24*). MATLAB's built-in GA was used during ocean testing, with populations of 10-20 individuals running for 10-20 generations. For ease of operation, we wrote our own GA in the Python programming language, which was used with populations of 15 individuals in laboratory tests.

When performing ocean testing, the robot was moved approximately six inches between tests to ensure burrowing occurred in virgin soil. Soil used in testing was always fully saturated and covered by seawater. The substrate used in laboratory testing was fully submerged in freshwater and contained within a 33 gallon industrial steel drum. The drum was vibrated by a commercial vibrator for 60 seconds between tests to relieve residual stresses in the substrate.

Accounting for variation in friction and sensor inaccuracy, energetic measurements made with RoboClam have an error of $\pm$ 15.6 J/m. Error in vertical position is $\pm$ 0.002 m.

Localized substrate failure during valve contraction

The effect that enables localized fluidization is failure in the soil. As *Ensis* contracts its valves, it reduces the level of stress acting between the valves and the surrounding substrate. At some stress level, the imbalance between the horizontal and vertical stresses causes the soil adjacent to the animal to fail. The failure zone is defined by a failure surface, outside of which soil remains stationary during contraction; within the failure zone, soil is allowed to freely move

with pore fluid, becoming fluidized.

Figure S3A shows a Mohr's circle representation of the effective stress states in a bed of soil at equilibrium and active failure (*6, 15*). Effective stress is the actual stress acting between soil particles, neglecting hydrostatic pressure of the pore fluid. The term "active" corresponds to the reduction of one of the principal stresses to induce failure (*6*). When *Ensis* first starts to contract, it relieves the stress acting between the substrate and its valves. At this point, the soil will tend to naturally landslide downward at a failure angle θ_f. The failure angle is the transformation angle between the principle stress state and the stress state at failure, where the applied stress (represented by the circle) equals the strength of the soil (represented by the failure envelope which is dictated by the friction angle ϕ). This angle can also be determined by connecting the tangency point on the stress envelope, the horizontal failure effective stress σ'_{hf}, and the principle stress axis, as shown in Fig. S3A and given by Eq. S2.

$$\theta_f = 45^\circ + \frac{\phi}{2}. \tag{S2}$$

To describe soil failure in three dimensions, *Ensis* can be modeled as a cylinder with contracting radius that is embedded in saturated soil, as shown in Fig. S3B. To neglect end effects, *Ensis* is modeled as an infinitely long cylinder. When *Ensis* initiates valve contraction, it induces changes in soil stress that cause incipient failure without yet moving the substrate particles. As this relaxation in pressure can be considered quasi-static and elastic (*6*), stresses due to inertial effects can be ignored and the total radial and hoop stress distribution in the substrate can be described with the thick-walled pressure vessel equations in Eqs. S3 and S4 (*25*), which have been modified to geotechnical conventions (with compressive stresses positive) and to reflect an infinite soil bed in lateral directions:

$$\sigma_r = \frac{R_0^2(p_i - p_0)}{r^2} + p_0 \tag{S3}$$

$$\sigma_\theta = -\frac{R_0^2(p_i - p_0)}{r^2} + p_0. \tag{S4}$$

In Eqs. S3 and S4, σ_r is total radial stress, σ_θ is total hoop stress, R_0 is *Ensis'* expanded radius (before contraction), p_i is the pressure acting on the animal's valves, and p_0 is the natural lateral equilibrium pressure in the soil. It is important to note that these equations still hold if there is a body force acting in the z-direction, such as in soil. In this case, the pressure vessel equations describe the state of stress within annular differential elements stacked in the z-direction, and total vertical stress is given as

$$\sigma_z = \rho_t g h \tag{S5}$$

where h is the clam's depth beneath the surface of the soil, ρ_t is the total density of the substrate (including solids and fluids), and g is the gravitational constant. It should be noted that there are no shear stresses within the soil in principal orientation, as $\tau_{rz} = \tau_{\theta z} = 0$ because our *Ensis* is modeled as infinitely long and there are no shear stresses acting on the soil surface, and $\tau_{r\theta} = 0$ because of symmetry.

The undisturbed horizontal effective stress is determined by subtracting hydrostatic pore pressure, u, from the natural lateral equilibrium pressure in the soil:

$$\sigma'_{h0} = p_0 - u. \tag{S6}$$

The undisturbed horizontal and vertical effective stresses can be correlated through the coefficient of lateral earth pressure

$$K_0 = \frac{\sigma'_{h0}}{\sigma'_{v0}} \tag{S7}$$

which is a measured soil property (*6, 27*). By also knowing the void fraction of the soil, ϵ, and the particle and fluid density, ρ_p and ρ_f respectively, p_0 can be determined with Eq. S8.

$$p_0 = K_0 \sigma'_{v0} + u = K_0 g h (1 - \epsilon)(\rho_p - \rho_f) + \rho_f g h. \tag{S8}$$

Failure of the substrate will occur when p_i is lowered to a point where the imbalance of two principle effective stresses produces a shear stress that exceeds the shear strength of the soil.

This resolved failure shear stress can be created by an imbalance between radial and vertical or radial and hoop stresses. In either case, active failure results in the same manner as shown by circle "b" in Fig. S3A. From the geometry of the circle and the failure envelope defined by ϕ, the relationship between stresses at failure for either mechanism can be defined as

$$\frac{\sigma'_{rf}}{\sigma'_{vf}} = \frac{\sigma'_{rf}}{\sigma'_{\theta f}} = \frac{1-\sin\phi}{1+\sin\phi} = K_a \tag{S9}$$

where subscript f denotes the stresses at failure and K_a is referred to as the coefficient of active failure. It is important to note that this failure analysis is also valid for cohesive soils. The one difference is that the failure envelope for a cohesive soil does not pass through (0,0) on a Mohrs circle, as cohesive stresses give soil shear strength even when no compressive stresses are applied. At sufficient depths the failure envelope can be approximated as running through (0,0) for any soil type, as compressive stresses due to gravity will dominate cohesive stresses.

Soil failure due to an imbalance between radial and vertical stresses will occur when the applied radial effective stress equals the radial stress at failure. The radial location of the failure surface in this condition, $R_{f_{rv}}$, given by Eq. S10, can be found by combing Eq. S3 for radial stress with Eqs. S6, S7, and S9, and realizing that the vertical effective stress at failure and equilibrium is unchanged. Hence failure occurs when:

$$\begin{aligned} \sigma'_r &= \sigma'_{rf}|_{r=R_{f_{rv}}} \\ \frac{R_0^2(p_i-p_0)}{r^2} + p_0 - u &= K_a\sigma'_{v0} = \frac{K_a}{K_0}(p_0-u) \end{aligned}$$

yielding the following expression for the dimensionless failure radius:

$$\frac{R_{f_{rv}}}{R_0} = \left[\frac{p_i-p_0}{\left(\frac{K_a}{K_0}-1\right)(p_0-u)}\right]^{\frac{1}{2}}. \tag{S10}$$

If soil failure is caused by the imbalance between radial and hoop stresses, the radial location of the failure surface, $R_{f_{r\theta}}$, can be found by combining Eqs. S3 and S4 for both stresses with

Eqs. S6 and S9 to produce Eq. S11:

$$\begin{aligned} \sigma'_r &= \sigma'_{rf}|_{r=R_{f_{r\theta}}} \\ \frac{R_0^2(p_i - p_0)}{r^2} + p_0 - u &= K_a\sigma'_{\theta f} = K_a\left(-\frac{R_0^2(p_i - p_0)}{r^2} + p_0 - u\right) \end{aligned}$$

yielding

$$\frac{R_{f_{r\theta}}}{R_0} = \left[\frac{(K_a + 1)(p_i - p_0)}{(K_a - 1)(p_0 - u)}\right]^{\frac{1}{2}}. \tag{S11}$$

The dominant failure mechanism in the soil surrounding a contracting cylindrical body is determined by the type of failure (radial-vertical or radial-hoop) that results in the largest failure surface radius. The ratio of failure radii for both mechanisms can be calculated by combining Eqs. S10 and S11 into Eq. S12.

$$\frac{R_{f_{rv}}}{R_{f_{r\theta}}} = \left[\frac{K_a - 1}{(K_a + 1)\left(\frac{K_a}{K_0} - 1\right)}\right]^{\frac{1}{2}}. \tag{S12}$$

Using values for real soils in Eq. S12, with K_a = 0.19 to 0.52 and K_0 = 0.31 to 1 (*6, 27*), yields $\frac{R_{f_{rv}}}{R_{f_{r\theta}}} \approx 1$ in most regions, with upper limits around 12. This result indicates that the failure radius created by both mechanisms is approximately the same size, with bias towards radial-vertical in some conditions. As such, Eq. S10 is used to predict scaling of the failure zone. If during contraction, p_i is assumed to be approximately zero, corresponding to complete stress release between *Ensis'* valves and the surrounding soil, and $\frac{K_0 p_0}{p_0 - u} \approx 1$ because K_0 is often around 0.5 and $u \approx 0.5p_0$, Eq. S10 can be simplified to Eq. S13:

$$\frac{R_f}{R_0} \approx (K_0 - K_a)^{-\frac{1}{2}}. \tag{S13}$$

This facilitates a prediction of R_f using only two soil properties, K_a and K_0, both of which are typically measured during a geotechnical survey (*26*).

Applying the range of possible K_a and K_0 values to Eq. S13 yields $1 < \frac{R_f}{R_0} < 4$ in most conditions. These results demonstrate that soil failure around a contracting cylindrical body is a relatively local effect, and for reductions of p_i near zero, depth-independent.

Figure captions for supporting online material

Figure S1: *Ensis* burrowing visualization system. A) Visualization tank filled with 1mm soda lime glass beads. Viewing panes are adjustable via lead screws to match tank and animal width, forcing a plane strain condition. Labeled regions: float valve (FV); accumulator (A); lead screw (LS); 500W halogen light (L); bellowed sidewall (B); and substrate (S). B) Example image of illuminated visualization tank with *Ensis* clearly seen in silhouette. C) Flow diagram of the visualizer's cooling and recirculation system. Chilled water, fed by gravity from a commercial lobster tank (LT), is mixed with warm water from the visualizer and fed into a pump (P). Water is pumped into the accumulator, which maintains level in the visualizer via a float valve. The outlet from the accumulator feeds both the visualizer and a short circuit line back to the lobster tank. As the resistance through the visualizer, R_V, is much less than the short circuit line resistance, R_L, nearly all of the water flowing from the pump is fresh from the lobster tank. The system is able to maintain 2°C difference between the visualizer and lobster tank with two halogen lights illuminated.

Figure S2: RoboClam's end effector. A) Functional parts of the end effector and packaging to prevent soil from entering the mechanism. B) Free body diagram of the end effector during expansion/contraction.

Figure S3: Soil failure around contracting *Ensis*. A) Mohr's circle representation of equilibrium (a) and active failure (b) stress states in a soil. Symbols: τ is shear stress; σ is normal stress; ϕ is the soil's friction angle; θ_f is the failure angle, corresponding to the landslide shear surface orientation; superscript $'$ denotes effective stress, the actual stress between substrate particles without the contribution of pore water hydrostatic pressure; subscript h indicates horizontal stress; subscript v indicates vertical stress; subscript 0 indicates equilibrium state; and subscript

f indicates failure state. B) Simplified, cylindrical model of soil failure around contracting *Ensis*. As *Ensis* contracts its valves, it reduces the pressure acting between its body and the soil, p_i, below that of the equilibrium lateral soil pressure, p_0. This stress imbalance induces a localized failure zone around the animal. Labels: r, z, and θ denote the cylindrical coordinate system; h is *Ensis'* depth in the substrate; L and R_0 are the animal's length and expanded radius, respectively; and R_f is the radius of the failure zone.

Figures for supporting online material

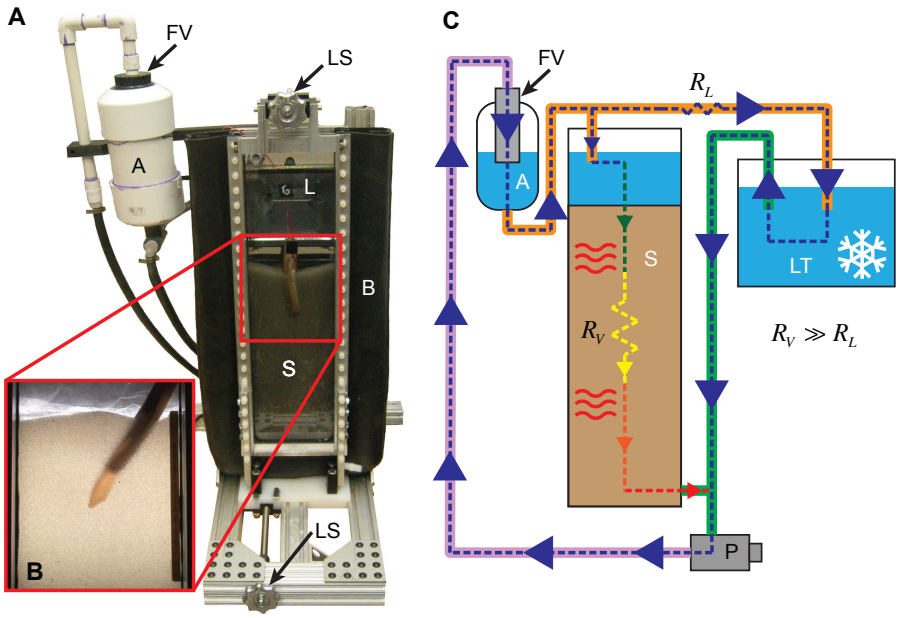

Figure S1: *Ensis* burrowing visualization system.

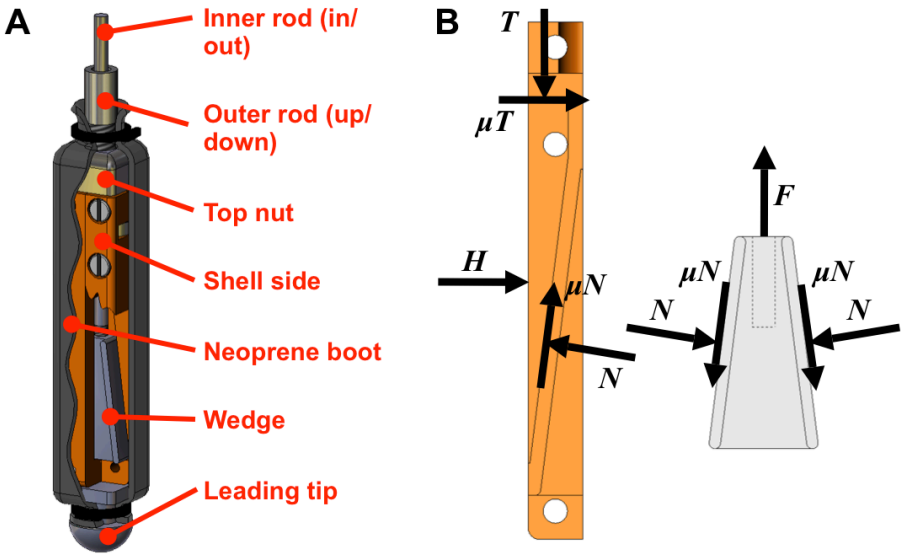

Figure S2: RoboClam's end effector.

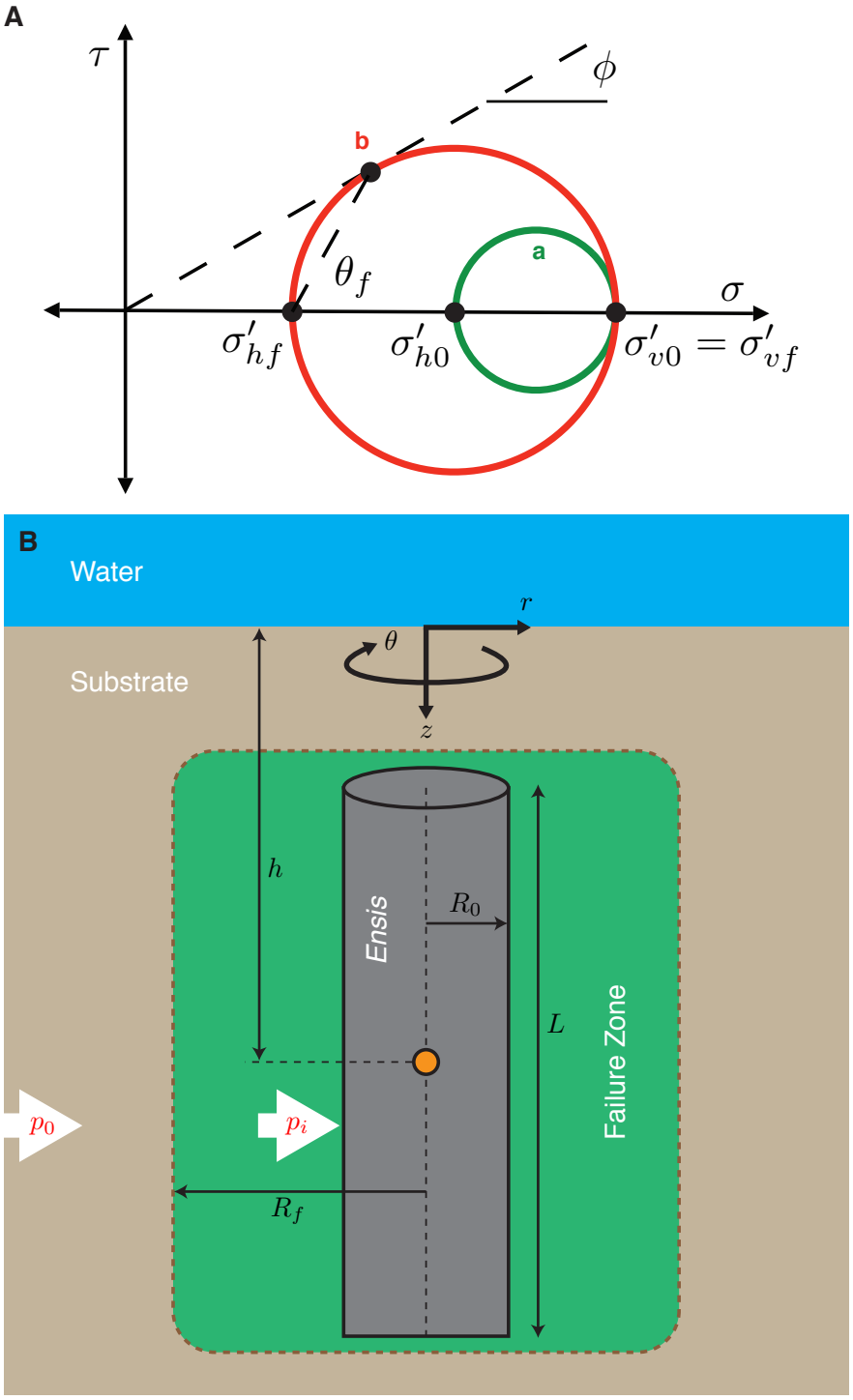

Figure S3: Soil failure around contracting *Ensis*.

International Journal of Non-Linear Mechanics ▮ (▮▮▮▮) ▮▮▮–▮▮▮

Contents lists available at ScienceDirect

International Journal of Non-Linear Mechanics

journal homepage: www.elsevier.com/locate/nlm

Dynamics of digging in wet soil

Sunghwan Jung [a,*], Amos G. Winter [b], A.E. Hosoi [b]

[a] Department of Engineering Science and Mechanics, Virginia Polytechnic Institute and State University, Blacksburg, VA 24061, USA
[b] Department of Mechanical Engineering, Hatsopoulos Microfluids Laboratory, Massachusetts Institute of Technology, Cambridge, MA 02139, USA

ARTICLE INFO

Keywords:
Bio-locomotion
Dynamics in wet soil
Atlantic razor clam

ABSTRACT

Numerous animals live in, and locomote through, subsea soils. To move in a medium dominated by frictional interactions, many of these animals have adopted unique burrowing strategies. This paper presents a burrowing model inspired by the Atlantic razor clam (*Ensis directus*), which uses deformations of its body to cyclically loosen and re-pack the surrounding soil in order to locally manipulate burrowing drag. The model reveals how an anisotropic body – composed of a cylinder and sphere varying sinusoidally in size and relative displacement – achieves unidirectional motion through a medium with variable frictional properties. This net displacement is attained even though the body kinematics are reciprocal and inertia of both the model organism and the surrounding medium are negligible. Our results indicate that body aspect ratio has a strong effect on burrowing velocity and efficiency, with a well-defined maximum for given kinematics and soil material properties.

1. Introduction

There are many examples of animals that live in particulate substrates which have evolved unique locomotion schemes [1]. Two common strategies observed in biological systems are an undulatory, snake-like motion [2–4,6] and a "two-anchor" system [5,7–12]. An example of the former is the sandfish lizard which wiggles its body from side to side in order to effectively swim through sand [2]. Similarly, smaller organisms like *C. elegans* have been observed to move quite efficiently via an undulatory motion through granular media [3,4]. In contrast, soft-bodied organisms that live in particulate substrates saturated with a pore liquid generally use a two-anchor system to burrow. In this strategy, one section of the animal expands to form a terminal anchor, while another section of the animal contracts to reduce drag. Once the contracted section is conveyed forward in the burrow, it is expanded to form the next terminal anchor and the previous terminal anchor is contracted and shifted forward.

The burrowing model presented in this paper is inspired by the two-anchor locomotion scheme and body geometry of the Atlantic razor clam (*Ensis directus*). *Ensis* is comprised of a long, slender set of valves (i.e. the two halves of the shell) which are hinged on an axis oriented longitudinally to the animal, and a dexterous soft foot which resides at the base of the valves. The burrowing cycle of *Ensis* is depicted in Fig. 1(a). The animal starts with its foot fully extended below the valves (A). Next, it uses a series of four shell motions to make downward progress: (B) the foot extends to uplift the valves while the valve halves contract to force blood into the foot, inflating it to serve as a terminal anchor; (C) the foot muscles contract to pull the valves downwards; and (D) the valves expand in order to form a terminal anchor and begin the cycle again.

The uplift and contraction motion of the valves draw water towards the animal's body, unpacking and locally fluidizing the surrounding substrate [13]. The initiation of valve contraction causes local soil failure around the animal and the uplift velocity is on the order of the pore fluid velocity required to induce a fluidized bed below the animal.[1] Although the animal is too weak to pull its shell through static soil (which exerts a resistance that linearly increases with depth [15]) to typical burrow depths, fluidization dramatically reduces drag, resulting in resistance forces that are depth independent [13]. The aim of this paper is to analyze the kinematic motion of the shell and demonstrate that reciprocal body deformations can produce unidirectional motion in a substrate of varying frictional properties.

2. Model

Fig. 1(b) shows the geometry of the simplified model organism and the dynamics inspired by *Ensis*. The body consists of two components: a long cylinder of length L and radius $r(t)$, which approximates the valves, and a sphere of radius $R(t)$ attached to the cylinder, acting as the foot. The radius of the cylinder, the radius of the sphere and the distance between the two are known functions of time dictated by the organism. The length of the shell, L, is considered constant.

* Corresponding author.
E-mail address: sunnyjsh@vt.edu (S. Jung).

[1] A full description of *Ensis* burrowing mechanics is beyond the scope of this paper, but can be found in [13].

0020-7462/$ - see front matter © 2010 Elsevier Ltd. All rights reserved.
doi:10.1016/j.ijnonlinmec.2010.11.007

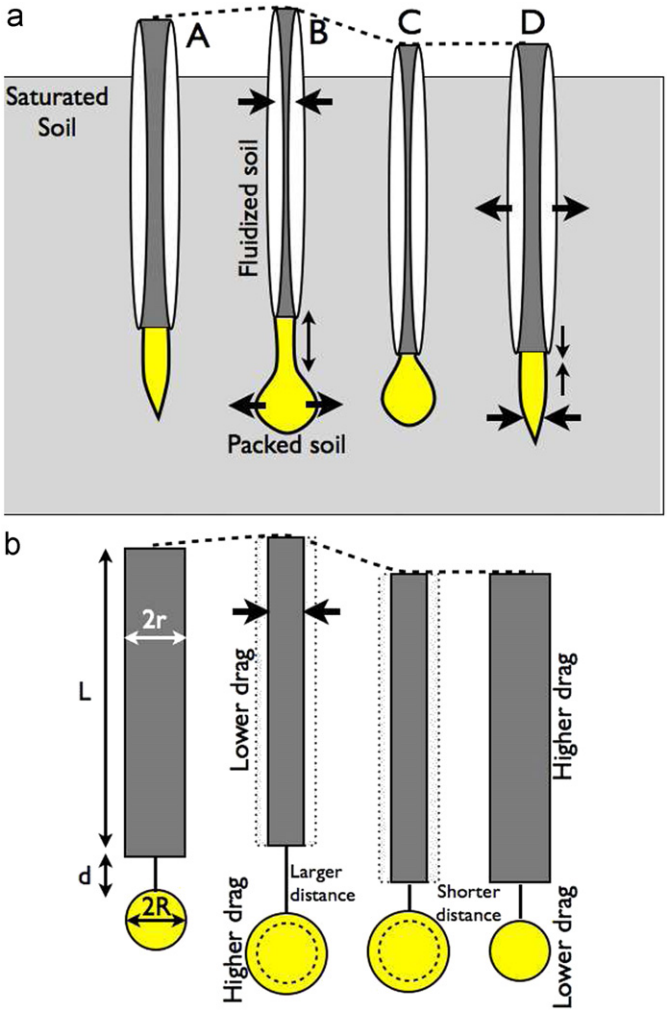

Fig. 1. Schematics of motion for (a) burrowing *Ensis* and (b) simplified model organism inspired by *Ensis*.

2.1. Kinematics

Ensis's burrowing motions are often erratic; the animal may wait anywhere from a few seconds [11] to many minutes between digging cycles. First, the radii of the cylinder and the sphere are given by

$$r = a_0 + a'\cos(\omega t), \quad R = a_0 - b'\cos(\omega t), \tag{1}$$

where ω is the frequency of motion and a_0 is chosen as the mean radius of both the cylinder and the sphere.

Another important factor in the kinematics of burrowing *Ensis* is the extension and retraction of the foot and its temporal relation to the movement of the valves. To model this motion, we impose a sinusoidally changing distance between cylinder and sphere that is out of phase with the expansions and contractions by $\pi/2$:

$$d = d_0 + d'\sin(\omega t). \tag{2}$$

2.2. Volume conservation

Delete "Recall that" In the live organism, the expansion of the foot is driven by fluid squeezed out of the shell. This fluid may be treated as incompressible at clam-like speeds and is contained in a closed loop. Hence, by conservation of volume, as the cylinder contracts, the sphere expands and vice versa. For small deformations, the change in the total volume of the cylinder can be approximated as

$$\dot{v}_{cyl} = 2\pi r\dot{r}L \sim -2\pi L\omega a_0 a'\sin(\omega t). \tag{3}$$

The sphere's volume varies with opposite phase and, again for small deformations is approximated as

$$\dot{v}_{sph} = 4\pi a_0^2\dot{R} \sim 4\pi\omega a_0^2 b'\sin(\omega t). \tag{4}$$

Combining these two relations and applying conservation of volume shows that the amplitude of the changing sphere radius is related to the deformations of the cylinder by $b' = (L/2a_0)\,a'$.

The initial mean void fraction of the surrounding medium, ε_0, is defined as the ratio of volume occupied by pore fluid to the total volume. The change in void fraction of the soil adjacent to the organism as the cylinder collapses relative to its mean value is given by

$$(\varepsilon_0 - \varepsilon)_{cyl} = \frac{\pi L(r^2 - a_0^2)}{\mathcal{V}_{cyl}} \sim \frac{2\pi L a_0}{\mathcal{V}_{cyl}} a'\cos(\omega t), \tag{5}$$

where $\mathcal{V}$ is the characteristic volume of the perturbed soil, the extent of which depends on the geometry of the burrowing organism and initial soil properties [13], and ε is the instantaneous local void fraction. In the same manner, the void fraction change in the soil surrounding the sphere is given by

$$(\varepsilon_0 - \varepsilon)_{sph} = \frac{4\pi}{3\mathcal{V}_{sph}}(R^3 - a_0^3) \sim -\frac{4\pi a_0^2}{\mathcal{V}_{sph}} b'\cos(\omega t). \tag{6}$$

2.3. Drag

The drag force on an object moving through a saturated particulate medium depends (non-linearly) on a number of parameters. In general, it can be written as

$$F_D = \mu(\varepsilon)V^\alpha S, \tag{7}$$

where μ is the resistance coefficient which depends on local void fraction ε, surface roughness, shape of the body, etc. V is the body's velocity, α is an exponent that varies with Reynolds number, and S is the geometric parameter that is associated with the body's contact area with the substrate. For Newtonian fluids, expressions for μ in the limits of both high and low Reynolds number flows are well known. The parameter α characterizes the velocity dependence in the drag expression. At high speeds (or high Reynolds numbers) the drag force is strongly dependent on velocity; however, as viscous effects increase and/or the substrate exhibits increasingly solid-like behavior, this velocity dependence weakens. For inviscid Newtonian flows, $\alpha = 2, \mu$ is related to the dimensionless drag coefficient, C_D, by $\mu = C_D\rho/2$ where ρ is the density of the fluid, and S is an effective cross-sectional area. At low Reynolds numbers, $\alpha = 1$ and μ is proportional to the dynamic viscosity of the fluid, μ_f where the constant of proportionality depends on the geometry of the body. For a sphere, $\mu = 6\pi\mu_f$ and S is the radius of the sphere.

It should be noted that the analysis presented in this paper is predicated on defining μf as an effective viscosity which correlates shear stresses to strain rate. This behavior is markedly different than critical state granular shear flow, where interparticle frictional interactions induce shear stresses that depend on confining pressure, and are relatively independent of strain rate [15]. Visualization of the fluidized substrate around burrowing *Ensis* show void fraction ranges of $0.42 < \varepsilon < 0.46$ [13], which is unpacked beyond the point of incipient fluidization ($\varepsilon \approx 0.41$) for uniform spheres [14]. As such, the substrate surrounding burrowing *Ensis* can be modeled with a fluid-like viscosity that is a function of void fraction, for which there are numerous empirically-derived expressions in the literature [18–21].

Please cite this article as: S. Jung, et al., Dynamics of digging in wet soil, Int. J. Non-Linear Mech. (2010), doi:10.1016/j.ijnonlinmec.2010.11.007

Following the sequence of events depicted in Fig. 1(b), inward (collapsing) motion of the cylinder increases the local void fraction and consequently decreases the resistive drag force on the cylindrical body. In contrast, the drag on the sphere (which expands as the cylinder collapses) increases as the cylinder collapses. Assuming small local changes in void fraction $\Delta\varepsilon = \varepsilon - \varepsilon_0$ about an initial ε_0, we can write the local resistance coefficient of the cylinder, $\mu_{cyl}(\varepsilon)$ as

$$\mu_{cyl}(\varepsilon) = \mu_{cyl}(\varepsilon_0) + \left.\frac{\partial \mu_{cyl}}{\partial \varepsilon}\right|_{\varepsilon_0} (\varepsilon - \varepsilon_0) + \cdots \equiv \mu_0 - \mu'_{cyl}\cos(\omega t), \tag{8}$$

where μ'_{cyl} can be written as a function of the geometry of the organism and the material properties of the substrate by substituting Eq. (5) into (8). In general, μ'_{cyl} is assumed to be less than μ_0 otherwise, the resultant negative drag on the moving body is not physical. For the sphere, μ_{sph} fluctuates out of phase with μ_{cyl} and is given by $\mu_{sph} = \mu_0 + \mu'_{sph}\cos(\omega t)$.

2.4. Burrowing velocity

For a freely moving body, the net linear and angular momentum on the body must be zero. Since we are considering an inertialess limit, the total force on the model organism equals zero at every instant in time. This condition enables us to calculate a net burrowing velocity of the cylinder/sphere system.

The only forces acting on the system are drag on the cylinder and drag on the sphere which must be equal and opposite:

$$\mu_{cyl}|V_{cyl}|^{\alpha} S_{cyl} = \mu_{sph}|V_{sph}|^{\alpha} S_{sph}. \tag{9}$$

Since the distance between the cylinder and the sphere, d, is prescribed by the digger, the two velocities must be related via a kinematic constraint: $\dot{d} = V_{cyl} - V_{sph}$, where the dot indicates a time derivative.

Solving for the velocity of the cylinder (which represents the shell of the digging clam) and substituting the kinematics defined in (2) we find the dimensionless digging velocity of the sphere, $\hat{V}_{sph} \equiv V_{sph}/(\omega d')$:

$$\hat{V}_{sph} = -\frac{\cos(\omega t)}{1+\gamma^{1/\alpha}}, \tag{10}$$

where

$$\gamma = \frac{1+(\mu'_{sph}/\mu_0)\cos(\omega t)}{1-(\mu'_{cyl}/\mu_0)\cos(\omega t)} \frac{S_{sph}}{S_{cyl}}. \tag{11}$$

Fig. 2 shows the relationship between this dimensionless burrowing velocity averaged over one cycle, $\overline{V}$, and the "shell" aspect ratio a_0/L with varying normalized perturbed resistance coefficient μ'/μ_0 and varying velocity dependence α. For simplicity, we have approximated $\mu'_{sph} = \mu'_{cyl} = \mu'$, and S_{cyl} and S_{sph} are chosen as $2\pi a_0 L$ and $4\pi a_0^2$, respectively. Note that as an approximation, choosing $\mu'_{sph} = \mu'_{cyl}$ is a reasonable first estimate but, in reality μ'_{sph} and μ'_{cyl} are dictated by the constitutive equation relating μ and ε (which can be quite complicated and is often determined empirically for soils) and the geometry of the digger.

Fig. 2 indicates that, for our chosen sinusoidal kinematics, the maximum burrowing velocity occurs at an aspect ratio of $a_0/L = 0.5$ regardless of the material properties of the soil. As the normalized perturbed resistance coefficient μ'/μ_0 is increased, the maximum velocity increases and, for small α, the velocity profile flattens out. These trends indicate that as the resistance becomes more sensitive to changes in void fraction the burrowing velocity increases. Fig. 3 shows a contour plot of burrowing velocity as a function of the normalized perturbed resistance coefficient μ'/μ_0 and α at the fastest aspect ratio $a_0/L = 0.5$. The burrowing velocity increases with decreasing dependence of body forces on local velocities and increasing perturbed resistance coefficient.

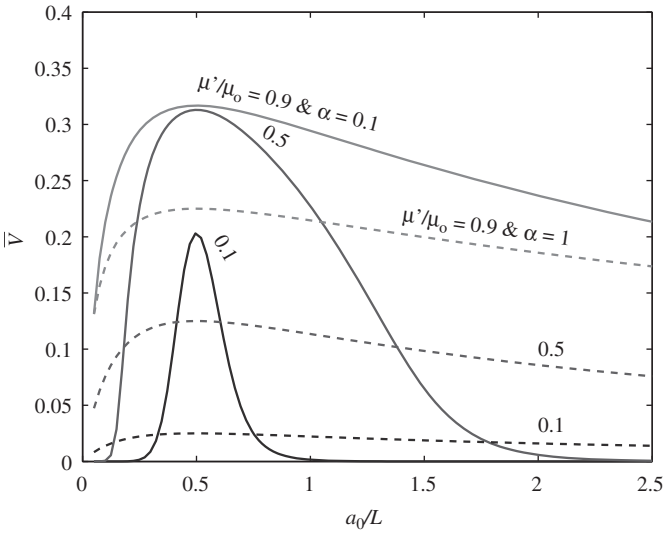

Fig. 2. Normalized burrowing velocity versus aspect ratio a_0/L with different normalized soil parameters μ'/μ_0. Dashed lines indicate $\alpha = 1$ (strong dependence on velocity) and solid lines correspond to $\alpha = 0.1$ (weak dependence on velocity).

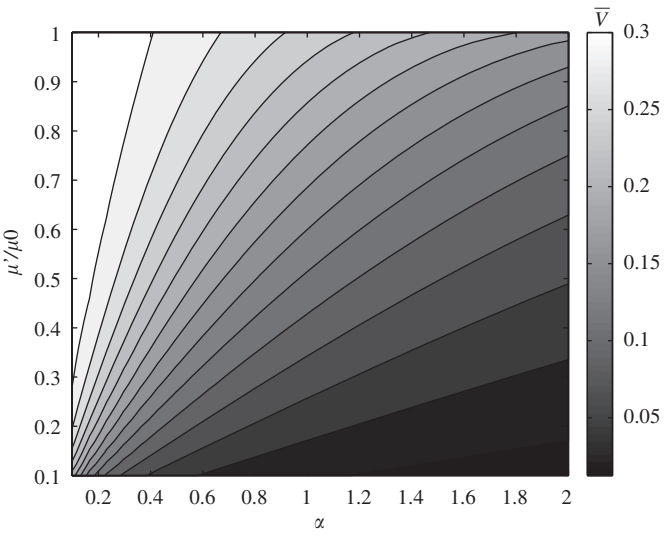

Fig. 3. A contour plot of maximum normalized velocity $\hat{V}_{cyl}$ time averaged over one cycle as a function μ'/μ_0 and α at the optimal aspect ratio, $a_0/L = 0.5$.

2.5. Efficiency

An actively burrowing animal consumes power as it deforms the surrounding medium and a certain fraction of that power is transformed into useful unidirectional motion. A typical hydrodynamical efficiency can be defined as the ratio of the power required to drag the digger through the soil at the average digging velocity (namely the useful fraction of the power) to the total power required to deform the substrate which can be expressed as

$$\eta = \mu_0 \frac{\overline{V}^{\alpha+1}(S_{cyl}+S_{sph})}{\sum_{i=sph,cyl} F_D^{(i)} \cdot V_i + P_i}, \tag{12}$$

where overline indicates a time-averaged quantity and the latter two terms in the denominator, P_{cyl} and P_{sph}, indicate the power dissipated by an expanding (or shrinking) cylinder and sphere, respectively. To evaluate the power associated with expansion,

Please cite this article as: S. Jung, et al., Dynamics of digging in wet soil, Int. J. Non-Linear Mech. (2010), doi:10.1016/j.ijnonlinmec.2010.11.007

we first calculate the corresponding stresses as $\sigma_{sph} = 2\mu_f \partial \dot{R}/\partial r = (4/3)\mu_f \dot{v}_{sph}/v_{sph}$ and $\sigma_{cyl} = 2\mu_f \partial \dot{r}/\partial r = \mu_f \dot{v}_{cyl}/v_{cyl}$, where v is the volume of the object and $\dot{v}$ is a dilation rate. As before, μ_f is the dynamic viscosity of the surrounding medium which is proportional to our resistance coefficient at low Reynolds numbers. The power dissipated is then given by $\sigma \dot{v}$ or

$$P_{sph} = \frac{4\mu_f}{3v_{sph}} \dot{v}_{sph}^2,$$

$$P_{cyl} = \frac{\mu_f}{v_{cyl}} \dot{v}_{cyl}^2. \tag{13}$$

Using Eqs. (3) and (4) and approximating the normalized perturbed soil parameter as the same as the normalized perturbed radius ($a'/a_0 = \mu'/\mu_0$), we can evaluate the power dissipated in expansion and contraction and compute the efficiency of digging. Note that this approximation only considers the dissipation associated with viscous stresses generated by an expanding object and at high Reynolds numbers there are additional components associated with P_i.

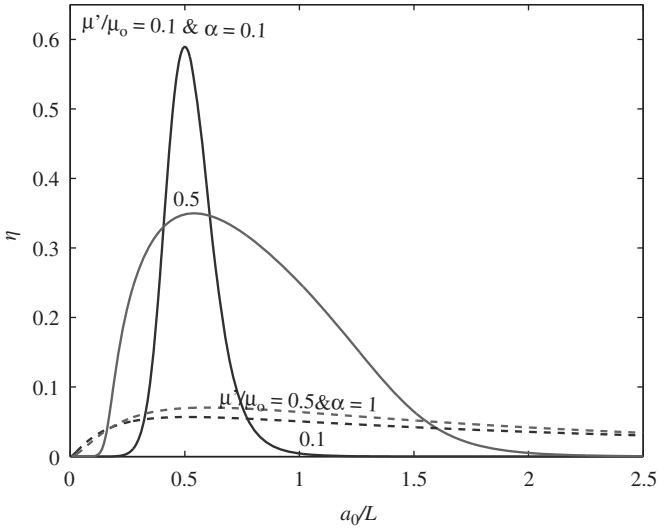

Fig. 4. Efficiency versus aspect ratio a_0/L with varying normalized soil parameters μ'/μ_0. Solid lines indicate $\alpha = 0.1$ (weak velocity dependence) and dashed lines correspond to $\alpha = 1$ (strong velocity dependence).

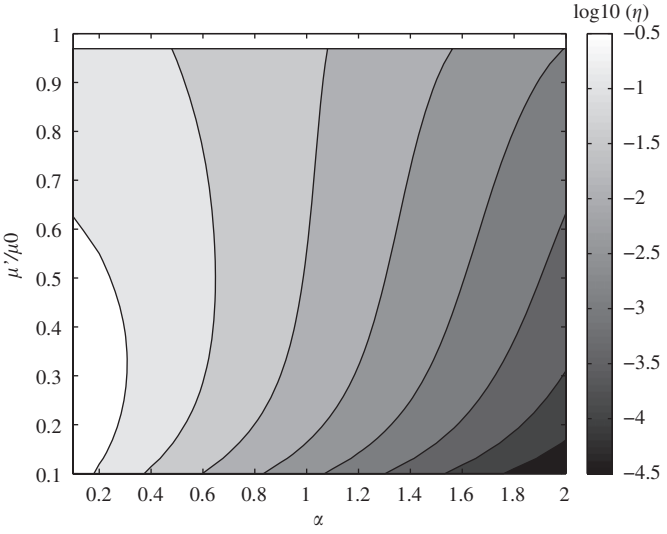

Fig. 5. A contour plot of efficiency η as a function μ'/μ_0 and α with $a_0/L = 0.5$.

Fig. 4 shows the efficiency as a function of aspect ratio a_0/L. When either the cylinder or the sphere undergoes a large variation in size, the local viscosity fluctuates significantly, increasing the burrowing velocity. However, these large deformations also dissipate a considerable amount of energy and hence, in contrast to the velocity, the efficiency *decreases* as the normalized perturbed soil parameter increases. In addition, larger normalized perturbed resistance coefficients broaden the efficiency profile as a function of a_0/L. Fig. 5 shows a contour plot of the efficiency as a function of α and μ'/μ_0 at the optimal aspect ratio, $a_0/L = 0.5$. At small α, the efficiency is large owing to the corresponding high burrowing velocity. This high efficiency rapidly drops as α increases and varies weakly in the normalized perturbed resistance coefficient.

To compare this with other animals locomoting in a fluid environment, the hydrodynamic efficiency is roughly 0.01 for small micro-organisms in a viscous fluid, and about 0.5 for large swimming animals in an unbounded fluid. Our results indicate that burrowing animals have relatively high efficiencies despite the large resistivity of their surrounding environments.

3. Discussion

Given this formulation, there are a number of limiting cases that can be addressed analytically, yielding further insight into optimal geometries for burrowing.

3.1. Limiting case 1: Small resistance perturbations

In the limit $\mu'/\mu_0 \ll 1$, we can estimate $\gamma^{1/\alpha}$ to first order in μ'/μ_0 as

$$\gamma^{1/\alpha} \sim \left(\frac{S_{sph}}{S_{cyl}}\right)^{1/\alpha} \left(1 + \frac{2}{\alpha}\frac{\mu'}{\mu_0}\cos(\omega t)\right), \tag{14}$$

where we have again approximated $\mu'_{cyl} \approx \mu'_{sph} \equiv \mu'$. Combining this with Eq. (10), we find the dimensionless instantaneous digging velocity can be represented as

$$\hat{V}_{sph} \sim \frac{1}{f}\left[1 - \frac{2}{\alpha}\frac{\mu'}{\mu_0}\frac{f-1}{f}\cos(\omega t)\right]\cos(\omega t),$$

where $f(a_0/L) = 1 + (S_{sph}/S_{cyl})^{1/\alpha}$. The mean dimensionless digging velocity of the clam, namely $\hat{V}_{sph}$ time-averaged over one cycle, is given as

$$\overline{V} = \frac{\omega}{2\pi}\int_0^{2\pi/\omega} V_{sph}\, dt \sim \frac{1}{\alpha}\frac{\mu'}{\mu_0}\frac{1-f}{f^2}. \tag{15}$$

Since $f \geq 1$, the body burrows downward in the vertical direction.

In order to maximize digging velocity for a given geometry we set

$$0 = \frac{\partial \overline{V}}{\partial (S_{sph}/S_{cyl})} \propto \frac{f-2}{f^3} \tag{16}$$

indicating that the maximum burrowing velocity occurs when $f = 2$ or equivalently when $S_{sph} = S_{cyl}$ regardless of the value of α or μ'. Thus, with $S_{cyl} = 2\pi a_0 L$ and $S_{sph} = 4\pi a_0^2$ the maximum velocity occurs at $a_0/L = 0.5$. However, this optimal aspect ratio depends on our choice of S, which depends on the details of the burrowing system.

3.2. Limiting case 2: Low Reynolds number Newtonian flows

As the Reynolds number approaches zero, forces acting on the bodies are linearly proportional to velocity ($\alpha = 1$). Expressions for these forces can be derived analytically, in particular, for an infinitely long cylinder aligned with the flow, the drag force is given by $2\pi\mu_f VL$ and the drag force on a sphere is given by $6\pi\mu_f V a_0$.

Please cite this article as: S. Jung, et al., Dynamics of digging in wet soil, Int. J. Non-Linear Mech. (2010), doi:10.1016/j.ijnonlinmec.2010.11.007

We again consider the limit of small resistance perturbations μ' due to local changes in particle packing fraction in a viscous fluid.

The calculation is the same as the previous calculation with the exception that $S_{sph}= a_0$ and $S_{cyl}=L/3$. Hence the corresponding burrowing velocity is maximized at $a_0/L=1/3$, corresponding to a more elongated cylinder than in the previous analysis.[2]

3.3. Near random close packing

For simplicity, our model has been linearized assuming small variations in the packing fraction. This reduced model provides a number of general insights into how reciprocal motion of non-symmetric bodies can generate unidirectional motion in a saturated soil. However, as the packing fraction of the substrate approaches critical transitional values (i.e. approaching random close packing), a fully nonlinear viscosity model is more appropriate.

There are a number of effective viscosity models which correspond to the special case of $\alpha=1$ associated with burrowing at low Reynolds numbers. A few such models relating the effective viscosity to the packing fraction, ϕ, are itemized in the table below.

μ/μ_f	References
$1+2.5\phi$	Einstein [18]
$1+2.5\phi+7.6\phi^2$	Batchelor and Green [19]
$(\frac{9}{8})\frac{(\phi/\phi_m)^{1/3}}{1-(\phi/\phi_m)^{1/3}}$	Frankel and Acrivos [20]
$\left(1-\frac{\phi}{\phi_m}\right)^{-\eta\phi_m}$	Krieger and Dougherty [21]

If we repeat the previous calculation to determine average digging velocities, this time taking into account the full nonlinear dependence cited in [21] and using typical parameters ($\eta=2.5$, $\phi_m=0.67$), the resultant velocity becomes $\overline{V}=0.1295$, which is commensurate with the values predicted by the linearized theory.

3.4. Previous numerical results

While to the best of our knowledge this paper represents the first theoretical analysis of a simple burrower using local fluidization to propel itself, this type of digging strategy has previously been studied numerically by Shimada et al. [17]. In that study, the authors used an event-driven granular simulation to model a "pushme–pullyou" consisting of two expanding and contracting disks separated by a spring. Both halves of the body were disks, hence aspect ratio was not a parameter in their study. In both studies (present and previous numerics) the burrowing velocity was found to be proportional to ω at low frequencies. In the event-driven simulations, the authors found that this relation peaks at a critical frequency and the velocity declines beyond this critical value. Our current theory is unable to predict these non-linearities observed at high ω on account of the assumptions made in the constitutive relationships, namely $\mu\propto\varepsilon$. A more realistic constitutive model (which would depend on the details of soil type, preparation, etc.) is likely to exhibit behavior that is qualitatively similar to the numerical simulations at high frequencies.

3.5. Conclusions

In this paper, we introduce a simple theoretical model to capture key physical aspects of burrowing *Ensis* and other biological or engineered burrowing systems. Even though the cylinder and sphere motion is actuated reciprocally in an over-damped environment, net unidirectional motion is achieved because of varying drag on the bodies owing to local changes in void fraction. We find that burrowing velocities depend on the aspect ratio, a_0/L, and that the "best" aspect ratio (i.e. the one that maximizes the velocity or the efficiency) depends on the geometric details of the drag force expression. It is interesting to note that while we found an optimal ratio of 1/3 for viscously dominated substrates, live razor clams have an aspect ratio closer to $a_0/L \sim 1/6$. This discrepancy is likely to arise due to an over-simplification of the constitutive relationships describing the substrate or may be an indication that razor clams have not evolved to maximize digging speeds. To better describe the dynamics of *Ensis*, future work will focus on more precisely determining the parameters and ε dependence in the force relation expressed in Eq. (7) and investigating other cost functions.

[2] Note that there is a subtlety in this calculation that needs to be addressed. The previous calculation, which should also be relevant at low Reynolds numbers, yielded an optimal aspect ratio of 1/2, not 1/3. To rationalize this apparent discrepancy, consider the drag on a sphere in a low Reynolds number flow. There are two common (and equivalent) ways to express the drag force: $F_D=6\pi\mu_f Va_0$ or $F_D=C_D\rho/2V^2S$, where $C_D=24/Re$ and $S=\pi a_0^2$. In the first case, in our formulation, we set $\mu=6\pi\mu_f$ and $S_{sph}=a_0$ resulting in an optimal aspect ratio of 1/3. In the second, we set $\mu=C_D\rho/2$ and $S_{sph}=S$ yielding an optimal aspect ratio of 1/2. To determine which is correct, we need to consider the constitutive relationship for the resistance coefficient. If $6\pi\mu_f$ can be well-approximated as a linear function of ε, the first formulation is relevant. If, on the other hand $C_D\rho/2=6\mu_f/(VR)$ (which includes the geometric parameter R which also affects the void fraction) can be considered a linear function of ε, the second estimate is more appropriate.

References

[1] E.R. Trueman, The Locomotion of Soft-Bodied Animals, J.W. Arrowsmith Ltd., Bristol, UK, 1975.
[2] R.D. Maladen, Y. Ding, C. Li, D.I. Goldman, Undulaory Swimming in sand: subsurface locomotion of the sandfish lizard, Science 325 (2009) 314–318.
[3] H.R. Wallace, The dynamics of nematode movement, Annu. Rev. Phytopathol. 6 (1968) 91–114.
[4] S. Jung, *Caenorhabditis elegans* swimming in a saturated particulate system, Phys. Fluids 22 (2010) 031903.
[5] E.W. Fager, Marine sediments: effects of a tube-building polychaete, Science 143 (3604) (1964) 356–359.
[6] M.D Kelly, et al., Burrow extension by crack propagation, Nature 433 (7025) (2005) 475.
[7] A.F. Holland, J.M. Dean, Biology of stout razor clam *Tagelus plebeius*. 1. Animal-sediment relationships feeding mechanism and community biology, Chesapeake Sci. 18 (1) (1977) 58–66.
[8] P.K.S. Shin, A.W.M. Ng, R.Y.H. Cheung, Burrowing responses of the short-neck clam *Ruditapes philippinarum* to sediment contaminants, Mar. Pollut. Bull. 45 (2002) 133–139.
[9] S.M. Stanley, Bivalve mollusk burrowing aided by discordant shell ornamentation, Science 166 (1969) 634–635.
[10] E.R. Trueman, Bivalve mollusks: fluid dynamics of burrowing, Science 152 (3721) (1966) 523–525.
[11] E.R. Trueman, The dynamics of burrowing in Ensis (Bivalvia), Proc. R. Soc. London Ser. B, 166 (1967) 459–476.
[12] E.R. Trueman, A.R. Brand, P. Davis, The dynamics of burrowing of some common littoral bivalves, J. Exp. Biol. 44 (1966) 469–492.
[13] A.G. Winter, V. Biologically inspired mechanisms for burrowing in undersea substrates. PhD Thesis in Mechanical Engineering, Massachusetts Institute of Technology, 77 Massachusetts Ave., Cambridge, MA 02139, September 2010.
[14] C.Y. Wen, Y.H. Yu, Mechanics of fluidization, Chem. Eng. Prog. Symp. Ser. 62 (1966) 100111.
[15] K. Terzaghi, R.B. Peck, G. Mesri, Soil Mechanics, third ed., John Wiley & Sons, New York, 1996.
[17] T. Shimada, D. Kadau, T. Shinbrot, H.J. Herrmann, Swimming in granular media, Phys. Rev. E 80 (2009) 020301.
[18] A. Einstein, Eine neue Bestimmung der Molekuldimensionen, Ann. Phys. 19 (1906) 289.
[19] G.K. Batchelor, J.T. Green, The determination of the bulk stress in a suspension of spherical particles to order c^2, J. Fluid Mech. 56 (1972) 401.
[20] N.A. Frankel, A. Acrivos, On the viscosity of a concentrated suspension of solid spheres, Chem. Eng. Sci. 22 (1967) 847.
[21] I.M. Krieger, T.J. Dougherty, A mechanism for non-Newtonian flow in suspensions of rigid spheres, Trans. Soc. Rheol. 137 (1959).

Please cite this article as: S. Jung, et al., Dynamics of digging in wet soil, Int. J. Non-Linear Mech. (2010), doi:10.1016/j.ijnonlinmec.2010.11.007

Proceedings of the ASME 2009 International Design Engineering Technical Conferences & Computers and Information in Engineering Conference
IDETC/CIE 2009
August 30 - September 2, 2009, San Diego, California, USA

DETC2009-87609

THE DESIGN AND TESTING OF A LOW-COST, GLOBALLY-MANUFACTURABLE, MULTI-SPEED MOBILITY AID DESIGNED FOR USE ON VARIED TERRAIN IN DEVELOPING AND DEVELOPED COUNTRIES

Amos G. Winter, V*
Department of Mechanical Engineering

Mario A. Bollini
Department of Mechanical Engineering

Danielle H. DeLatte
Department of Aeronautics and Astronautics

Harrison F. O'Hanley
Department of Mechanical Engineering

Natasha K. Scolnik
Department of Mechanical Engineering

MIT Mobility Lab
Massachusetts Institute of Technology, Cambridge, Massachusetts 02139, U.S.A.

ABSTRACT

Mobility aids that are currently available in developing countries do not fully meet users' needs. People require a device that is maneuverable within the home and that can travel long distances on rough roads. To address this problem, we have designed the Leveraged Freedom Chair (LFC), a wheelchair-based mobility aid capable of navigating virtually any terrain by optimally utilizing upper body power for propulsion through a variable-speed lever drivetrain. The lever system achieves a 4:1 change in mechanical advantage, equating to leverage that ranges from 0.42X to 1.65X a standard wheelchair hand rim. In comparative trials, the LFC demonstrated capabilities that far exceed those of any mobility aid currently available in the developing world; it was able to cruise on smooth surfaces at 2m/s (5mph), climb muddy, grassy hills with a 1:3 slope, and navigate terrain with a coefficient of rolling resistance as high as 0.48. This operational flexibility should make the LFC usable on any terrain, from rural walking paths to tight indoor confines, and greatly increase the mobility of people with disabilities in developing countries. The LFC may also be attractive to wheelchair users in developed countries, as its performance breadth exceeds that of currently available products.

1 INTRODUCTION

In this work we present the Leveraged Freedom Chair (LFC), a wheelchair-based mobility aid that can be made anywhere in the world with off-the-shelf bicycle parts and cope with varied terrain ranging from steep hills to sandy roads to muddy walking paths to within the home. The motivation behind this project is to provide mobility to people with disabilities in developing countries no matter their location, travel requirements, or local environment. A mobility aid that can meet these requirements is desperately needed, as 20 million people in the developing world require a wheelchair [1] but only about five percent actually have one [2]. Disability is both a cause and consequence of poverty [3]; 98% of children with disabilities in developing countries do not attend school [4], and lack of mobility can deny people essential social rights like having a job or participating in their community. Public transportation is rarely an option, as 70% of the developing world disabled live in rural areas [5]. Even if busses are available, people with disabilities in developing countries are often charged double to bring their wheelchair onboard or flat-out turned away because of discrimination [6].

The lack of alternative transportation means most mobility aid users have to travel under their own power to get from point A to B, often on harsh terrain for multiple kilometers [6]. Products that are currently available in developing countries can not fulfill the wide usage needs of the disabled. Conventional western-styled wheelchairs, as shown in Fig. 1a, are inefficient to propel [7] and are exhausting to use for long distances on rough roads. Imported wheelchairs usually contain parts that are impossible to replace once broken. Even locally-made products

* PhD Candidate and author of correspondence, Phone: (617) 312-4207, Email: awinter@mit.edu

rely on expensive bearings and custom components that raise the price to a level out of reach for most people in the developing world. Hand-powered tricycles (Fig. 1b), which are preferred if the user has adequate torso stability [6], are more efficient to propel than a wheelchair [7-9] and cost less due to the incorporation of standardized bicycle components. Unfortunately, tricycles are difficult to maneuver through sand and up steep hills, and are much too large to use within the home.

a. Wheelchair b. Hand-powered tricycle

Figure 1. Common developing country mobility aids

2 LEVERAGED FREEDOM CHAIR DESIGN

The LFC is designed to span the operational space between long-distance travel on rough roads and mobility in tight confines, such as in the home. This is accomplished through a lever drivetrain mounted on a three-wheeled wheelchair platform, as shown in Fig. 2. The lever system, which is discussed in the following sections, is designed to optimally convert upper body power for propulsion in a wide range of terrains. For short-range mobility, such as in an office or around a bathroom, the LFC can be converted to a conventional wheelchair by simply removing the levers. The wheel layout and rider position is derived from the Worldmade Wheelchair, designed by Motivation UK [10]. The Worldmade is a popular wheelchair in developing countries because its three wheels are always kinematically constrained with the ground. Its long wheelbase provides stability and decreases loading on the front wheel, which combined with its large diameter, increases comfort and ability to go over obstacles.

Figure 2. The Leveraged Freedom Chair

2.1 VARIABLE-SPEED, FIXED GEAR RATIO LEVER DRIVETRAIN

Imagine trying to ride a mountain bike off-road, using only one gear, and pedaling with your hands. This scenario is analogous to the trials faced by users of wheelchairs and tricycles in developing countries. Just as a multi-speed bicycle enables the user to maintain a relatively constant power output while riding on diverse terrain, a mobility aid intended for use on anything from muddy hills to smooth streets requires variable mechanical advantage. The LFC achieves a multi-speed, fixed gear ratio drivetrain with the lever system shown in Fig. 3.

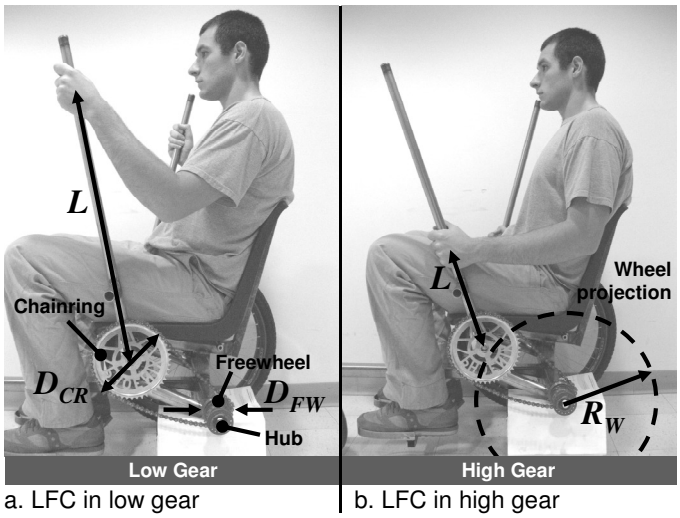

a. LFC in low gear b. LFC in high gear

Figure 3. Changing hand position on the levers varies mechanical advantage of the drivetrain

Unlike most gear trains, which operate in varied states to obtain multiple ratios, the LFC's drivetrain exists in only one state; it is the user who changes his hand position to change the mechanical advantage of the device. If more torque at the wheel is needed to climb a hill, the user simply slides his hands up the levers and away from the pivots, as shown in Fig. 3a. If more speed is required, the user moves his hands closer to the lever pivots, as shown in Fig. 3b, achieving a greater angular deflection with every push stroke. The relationship between chair speed and hand speed is represented by Eqn. 1

$$\frac{V_{Chair}}{V_{Hand}} = \frac{D_{CR} R_W}{D_{FW} L} \tag{1}$$

where V_{Chair} is the chair velocity, V_{Hand} is the user's hand velocity, D_{CR} is the chainring diameter, R_W is the wheel radius, D_{FW} is the freewheel diameter, and L is the lever length.

The fixed gear ratio offers a number of advantages over a multi-speed gear train. First, it does not require a derailleur, which is an expensive, unreliable, and fragile part in the developing world [11, 12]. Second, it enables the gear train to be lightweight. Third, all rolling elements are fabricated from bicycle parts that can be purchased in any developing country [12]. This means every moving part of the LFC is locally available and repairable by bicycle technicians. Finally, the use of bicycle parts makes the LFC inexpensive to produce; gear train parts for one chair cost $20US, which is approximately the same price as two rear hub and bearing sets used in East African-produced wheelchairs [13]. The expected total cost of the LFC is approximately $150-$400US, the same price range of wheelchairs currently produced in developing countries [14-16].

The LFC is powered by pushing the levers forward. On the return (pull) stroke, bicycle freewheels on the rear hubs allow the chains to freely ratchet and the levers to return to the starting position of the push stroke. This actuation scheme was chosen to enable people with a large range of disabilities to propel the LFC. For example, a person with a spinal cord injury may not have control of his abdominal muscles. The pushing motion allows the rider to brace against the seat back, whereas a pulling power stroke could pull him out of the chair. Furthermore, pushing levers engages larger muscle groups than using conventional hand rims, resulting in a greater power output with less exertion [7-9]. Braking is accomplished by pulling the levers close to the rider's body, past the starting angle of the push stroke. This forces the small tubes protruding orthogonally from the levers, which can be seen in Fig. 2, to contact the tires. The braking motion does not tend to push the rider out of the chair, as the seat recline angle allows body weight to aid in pulling on the levers. Steering of the LFC is accomplished by either differentially powering or braking the wheels.

2.2 LEVER GEOMETRY OPTIMIZATION

The design of the LFC gear train geometry was driven by human power capabilities. Available upper body pushing power for propulsion was determined by adapting results from Woude, et al [8], and was calculated to be 19.6W with a pushing force of 58N and hand velocity of 0.38m/s. In this paper, young men were tested to find the gear ratio for a lever-powered system that would yield the highest efficiency with relatively low exertion (approximately 30% increase in heart rate from resting). This level of power output was used in Eqn. 2 to calculate the attainable velocity for long-duration travel on a variety of terrains, neglecting efficiency losses in the drivetrain.

$$\begin{aligned} P_{Human} &= P_{Drag} + P_{Rolling} + P_{Gravity} \\ &= C_D \frac{1}{2} \rho_{air} A (V_{Chair})^3 \\ &\quad + mg(V_{Chair})[\mu_{roll} \cos\theta + \sin\theta] \end{aligned} \tag{2}$$

Values used in Eqn. 2 were C_D = 1 [17], ρ_{air} = 1.2kg/m^3, A = 0.6m^2, rider+chair mass m = 75kg, and g = 9.81m/s^2. Road surfaces in developing countries vary from tarmac to gravel to mud to sand, corresponding to rolling friction coefficients, μ_{roll}, ranging from 0.005 to 0.5 [17, 18]. Slope angles, θ, used in this analysis were varied between 0° and 40°, just beyond the backwards tipping angle of the LFC.

Using Eqn. 1 with V_{Hand} = 0.38m/s and the V_{Chair} data generated from Eqn. 2, the required lever length at each combination of rolling resistance and angle was computed. These data were compared to lever lengths that the authors could comfortably grasp, which were measured to be a maximum of L = 86cm to a minimum of L = 22cm. This comparison, shown in Fig. 4, demonstrates that for common road conditions, with rolling friction ranging from 0.01 to 0.1 (approximately tarmac to gravel) and slopes up to 5° (1:11 rise), the rider can propel himself at maximum efficiency. Expected velocities over these terrains, calculated with Eqn. 2, are plotted in Fig. 5.

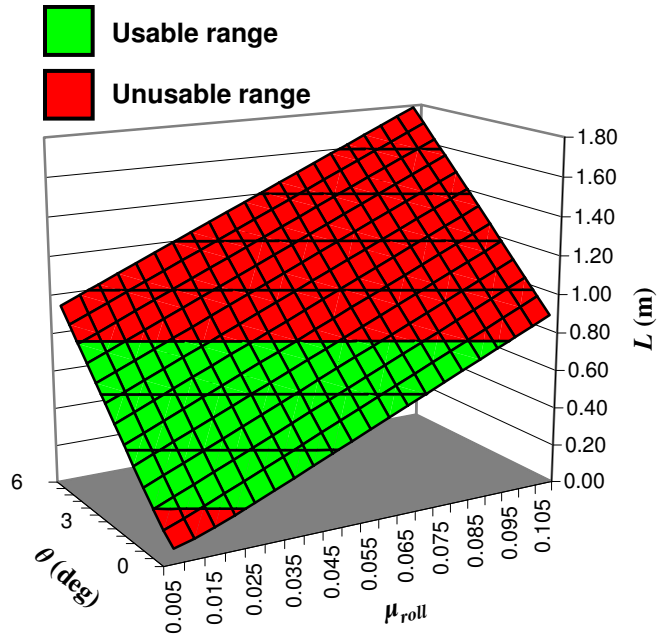

Figure 4. Required lever lengths for varying terrains at peak efficiency power output

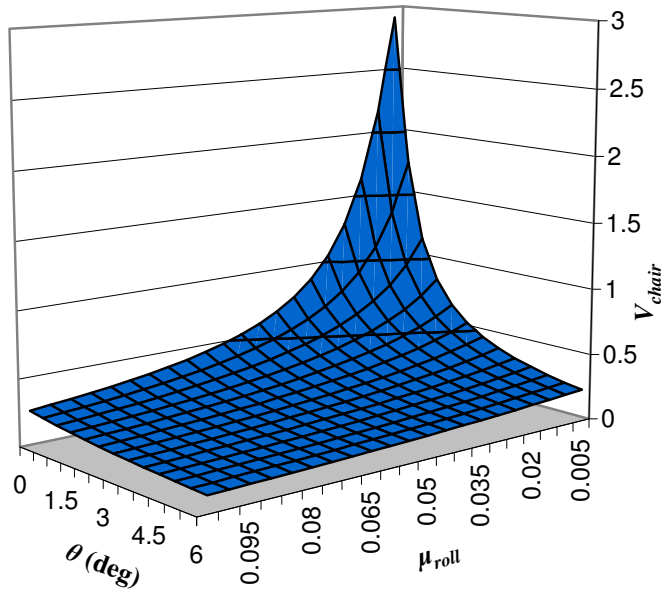

Figure 5. Attainable velocity at peak efficiency power output

On high resistance surfaces, such as sand or steep hills, an LFC rider may have to compromise efficiency in order to achieve high torque at the wheels. In these situations the chair velocity will be approximately zero, reducing Eqn. 2 to Eqn. 3,

$$F_{Resist} = mg\left[\mu_{roll}\cos\theta + \sin\theta\right] \tag{3}$$

where F_{Resist} is the total resistance force acting on the chair. Rearranging Eqn. 1 for force instead of speed transfer, and neglecting drivetrain efficiency, yields Eqn. 4,

$$\frac{F_{Resist}}{F_{Hand}} = \frac{D_{FW}L}{D_{CR}R_W} \tag{4}$$

where F_{Hand} is the pushing force exerted on the levers. By combining Equations 3 and 4, the required lever length for any terrain condition can be solved as a function of F_{Hand}.

Maximum attainable pushing force was determined through US military tests on aircraft control sticks [19] – an interface geometrically similar to the LFC levers. For males in the 50th percentile of the population, this force was measured to be 356N. Using F_{Hand} = 356N, the required lever length at every plausible operating point was computed, and is shown in Fig. 6.

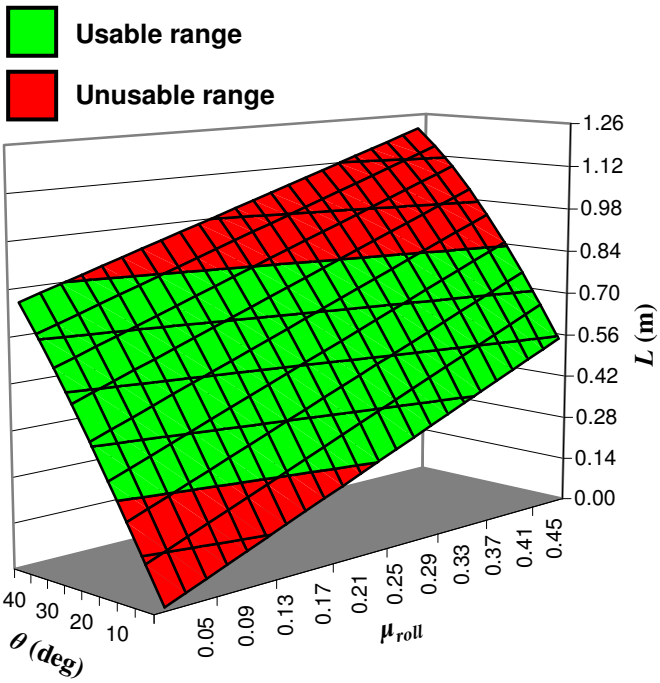

Figure 6. Required lever lengths for varying terrains at peak force output

The drivetrain configuration used to generate Figures 4-6 was composed of a 36-tooth chainring and a 20-tooth freewheel. The most common chainring sizes available in developing countries are 52, 48, 44, 36, and 32 teeth and the most common and robust freewheel size is 20 teeth [12]. The 36/20 chainring/freewheel combination was chosen because it maximized the operation range between high-speed and high-torque performance.

The results presented in Figures 4-6 demonstrate that one set of levers, which can be grasped between 22cm to 86cm from the pivot, will enable an LFC rider to travel on virtually any terrain. On common road surfaces, such as tarmac, gravel, and 5% grade slopes, the user will be able to efficiently cruise at high speed. When faced with off-road travel, the user will have the leverage to overcome harsh terrain like sand, mud, or 20% grade slopes. To further illustrate the breadth of the LFC's capability, the effective lever arm produced by the drivetrain

can be compared to a conventional wheelchair hand rim through an effective hand rim radius, *R'*, which is defined in Eqn. 5.

$$R' = \frac{LD_{FW}}{R_{HR}D_{CR}} \tag{5}$$

Eqn. 5 is plotted in Fig. 7 using R_{HR} = 29cm, the hand rim radius from the wheelchair in Fig. 1a, with the LFC's gear ratio and lever length range. Fig. 7 shows that the LFC drivetrain is able to vary by 4:1 in mechanical advantage, effectively producing a 0.42X to 1.65X hand rim.

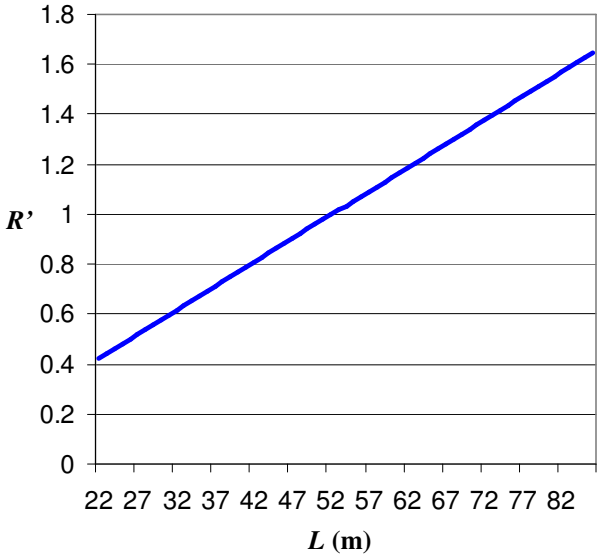

Figure 7. Effective hand rim radius vs. positions on LFC levers

3 LFC TESTING AND COMPARISON TO EXISTING MOBILITY AIDS

To compare the performance between the LFC and existing developing country mobility aids, the LFC was tested in various environments and operating conditions against the East African wheelchair and tricycle pictured in Fig. 1. The first trial was an endurance test on level, smooth terrain. Five test subjects, three male and two female, ranging from age 22-29, none regular wheelchair users, rode each mobility aid 0.87km (0.54miles) on a course through the MIT campus. The subjects were told to travel at a comfortable, relaxed pace that they could maintain throughout the trial. Average velocity and exertion, measured through increased heart rate (HR) from resting, was recorded for each subject and assembled into the chart in Fig. 8.

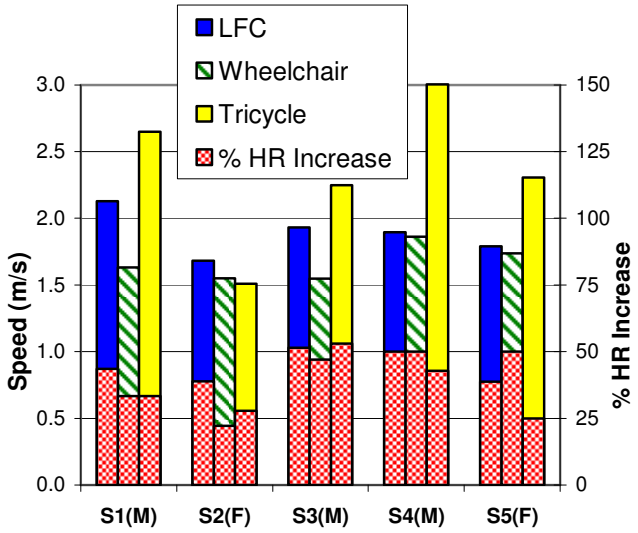

Figure 8. Average velocity and heart rate increase for long distance trials

The mean LFC velocity for the team was 1.89m/s, nearly the exact velocity predicted by Fig. 5 for flat, smooth terrain and moderate levels of exertion. The wheelchair was 11.7% slower with an average velocity of 1.67 m/s, and the tricycle was 24.3% faster at 2.34m/s. Percent increased heart rate from rest for the LFC, wheelchair, and tricycle were 44.5%, 40.5%, and 36.4%, respectively.

These results show that the LFC is faster than a wheelchair on flat, smooth surfaces for relatively the same amount of exertion, but looses out to the tricycle. Qualitatively, all of the test subjects reported that the LFC does not strain the shoulder muscles as much as the wheelchair. Additionally, the subjects found that they were able to add propulsion power to the LFC by engaging their abdominal muscles.

The second test was a hill climb trial to measure high power output performance. The hill used was a stepped, concrete indoor ramp composed of 1:12 slope sections, with an overall run of 42.1m and rise of 2.9m. The subjects rode each mobility aid up the ramp as fast as possible. Average velocity and increase in HR were recorded for each trial and compiled into Fig. 9.

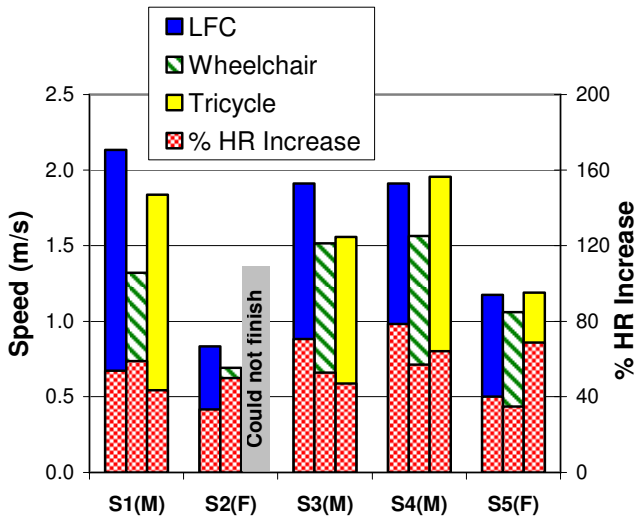

Figure 9. Average velocity and heart rate increase for hill climb trials

The LFC had the fastest team-averaged velocity up the ramp at 1.59m/s, with the wheelchair 22.7% slower at 1.23m/s and the tricycle 17.9% slower at 1.31m/s. The exertion levels for each mobility aid were similar, with increased heart rate from rest for the LFC, wheelchair, and tricycle 55.3%, 50.8%, and 55.9%, respectively. These results indicate that the LFC can deliver power at high resistances more efficiently than the other mobility aids. The wheelchair and tricycle could not produce as high mechanical advantage as the LFC, resulting in larger pushing forces, slower arm speed, and wasted metabolic power. The tricycle was geared so high that subject S2(F) could not make it up the ramp.

The final tests were conducted outdoors on ultra-high resistance surfaces in order to simulate the limits of what could be encountered in a developing country. Figure 10 shows the LFC traveling through snow, with a measured coefficient of rolling resistance that averaged from 0.21 to 0.34, with peaks as high as 0.48. The three subjects who tested the LFC in this condition were easily, although slowly, able to make progress over the ground by grasping high on the levers. Both the wheelchair and tricycle were impossible to propel through the snow. The wheelchair was geared too high, and the wet hand rims were too slippery to push effectively. The tricycle was also geared too high and did not have enough loading on the front wheel to maintain traction.

Figure 10. The LFC traveling on snow

Figure 11 shows the LFC climbing a 17.6° slope (1:3.1 rise) on wet, muddy grass. To put the formidability of this slope in perspective, the maximum allowable rise of a smooth wheelchair ramp is 1:12 according to ADA regulations [20].

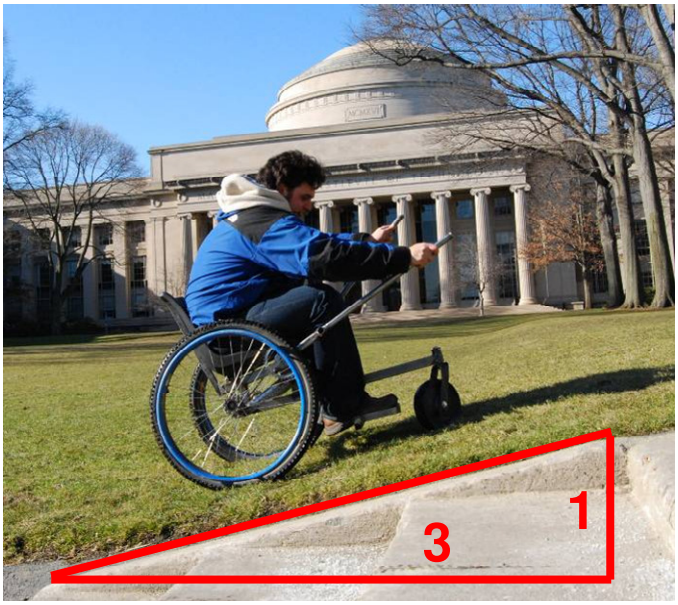

Figure 11. LFC going up 1:3 rise during hill climb trials

4 CONCLUSION AND FUTURE WORK

The LFC is a mobility aid that that is capable of traversing virtually any terrain encountered in developing countries. The variable mechanical advantage attained from the lever drivetrain enables an LFC user to travel quickly and efficiently on smooth, flat roads and produce enough torque to conquer steep hills and soft ground. The single-speed, bicycle component drivetrain allows the LFC to be built and serviced anywhere in the world at prices similar to existing mobility aids. Although some disabilities may prevent full utilization of the lever system, we are confident that the LFC will drastically increase the mobility of most people requiring a wheelchair in developing countries. Furthermore, the LFC has significant potential as a new product in developed countries, as its range of capabilities extend beyond those of any mobility aid currently available.

In August 2009 an updated LFC prototype will be taken to Africa for four-month long trials with the Association for the Physically Disabled of Kenya (APDK). This new version of the LFC will include a lightweight frame and a fully supportive wheelchair seat with cushion. Four prototypes will be manufactured with APDK and distributed to regions of Kenya with differing terrains. User feedback will be collected in January 2010 and used to refine the design. When the design is finalized we plan to start LFC production through APDK and other developing country wheelchair manufacturers.

ACKNOWLEDGMENTS

Funding for this project was provided by the Hugh Hampton Young Memorial Fund Fellowship, the MIT Department of Mechanical Engineering, the MIT IDEAS Competition, the MIT Public Service Center, and the MIT Undergraduate Research Opportunities Program. The authors would like to thank Dan Frey, Forrest Funnel, Ralf Hotchkiss, and Gwyndaf Jones for their assistance in designing, building, and testing the LFC, as well as the developing country wheelchair manufacturers who have aided in the development of this project: the Association for the Physically Disabled of Kenya, Nairobi, Kenya; The Kilimanjaro Association for the Spinally Injured, Moshi, Tanzania; the Mobility Care Wheelchair Workshop, Arusha, Tanzania; the MADE Wheelchair Workshop, Kampala, Uganda; and the Kien Tuong Wheelchair Workshop, Ho Chi Minh City, Vietnam.

REFERENCES

1. *Annual Program Statement.* USAID, 2003.
2. Warner, D., 1998, *Nothing About Us Without Us: Developing Innovative Technologies For, By and With Disabled Persons*.
3. *Issues Paper on Disability, Poverty and Development.* UK DFID, 2000.
4. *People with disabilities.* UNESCO Bangkok, 2003. **IV**(APPEAL).
5. Groce, N.E., 1999, *Health beliefs and behaviour towards individuals with disability cross-culturally.* Introduction to Cross-Cultural Rehabilitation: An International perspective.
6. Winter V, A.G., 2006, *Assessment of Wheelchair Technology in Tanzania.* The International Journal of Service Learning in Engineering, **1**(2): p. 60-77.
7. van der Woude, L.H.V., et al., 2001, *Alternative Modes of Manual Wheelchair Ambulation: An Overview.* American Journal of Physical Medicine & Rehabilitation, **80**(10): p. 765-777.
8. Woude, L.H.V.v.d., et al., 1997, *Mechanical Advantage in Wheelchair Lever Propulsion: Effect on Physical Strain and Efficiency.* Journal of Rehabilitation Research and Development, **34**(3): p. 286-294.
9. Linden, W.L.v.d., et al., 1996, *The Effect of Wheelchair Handrim Tube Diameter on Propulsion Efficiency and Force Application (Tube Diameter and Efficiency in Wheelchairs).* IEEE Transactions on Rehabilitation Engineering, **4**(3).
10. *Worldmade Wheelchair*, Motivation UK, http://www.worldmade.info/southafrica.html.
11. MIT, *Available bicycle parts in Tanzania*, Wheelchair Design in Developing Countries Class, http://web.mit.edu/sp.784/www/DOCUMENTS/Tanzania%20Components%20Price%20List.xls.
12. *Conversations with bicycle part suppliers in: Nairobi, Kenya; Dar es Salaam; Tanzania, Lusaka, Zambia; Antigua, Guatemala, and Chinandega, Nicaragua.* 2005-2009.
13. *Personal communications.* Mobility Care Wheelchairs, Moshi, Tanzania, 2005.
14. *Prices determined through personal communication.* Association for the Physically Disabled of Kenya, Nairobi, Kenya, 2008.
15. *Prices determined through personal communication.* Kien Tuong Wheelchair Workshop, Ho Chi Minh City, Vietnam, 2007.
16. *Prices determined through personal communication.* Transitions Wheelchair Workshop, Antigua, Guatemala, 2009.
17. Wilson, D.G., 2004, *Bicycling Science*. 3 ed., Cambridge, Massachusetts: MIT Press.
18. Avallone, E.A. and I. T. Baumeister, 1996, *Marks' Standard Handbook for Mechanical Engineers*. 10 ed., New York: McGraw-Hill, Chapt. 3, p. 25.
19. Cott, H.P.V. and R.G. Kinkade, 1972, *Human Engineering Guide to Equipment Design*, Washington D.C.: U.S. Government Printing Office.
20. ADA, 2002, *Accessibility Guidelines for Buildings and Facilities (ADAAG), 4.8 Ramps*, United States Access Board.

Global Design: Research, Innovation, and Eduction Focused on Emerging Markets

Amos Winter, PhD

Post-Doctoral Research Associate

SUTD-MIT International Design Center

Director, MIT Mobility Lab

MIT Mobility Lab (M-Lab)

- Students develop mobility-focused technology with stakeholders
- Partner with 15+ disability organizations around the world
- Learn how technical skills can make positive impact on world
- 80+ students involved, 20+ traveled abroad

The Leveraged Freedom Chair

Motivation behind the LFC

Disability in developing world

- 20 million people need a wheelchair but do not have one[1]
- 70% live in rural areas[2]
- Long distances on rough terrain to community connections

1. *Annual Program Statement,* USAID, 2003.
2. Groce, N.E., *Health beliefs and behavior towards individuals with disability cross-culturally,* 1999

Problems with current tech

Existing products do not fully provide mobility

- Wheelchairs are difficult to propel off road
- Tricycles are too big to use in the home

LFC usage requirements

LFC drivetrain innovation

Fixed gear ratio, variable speed

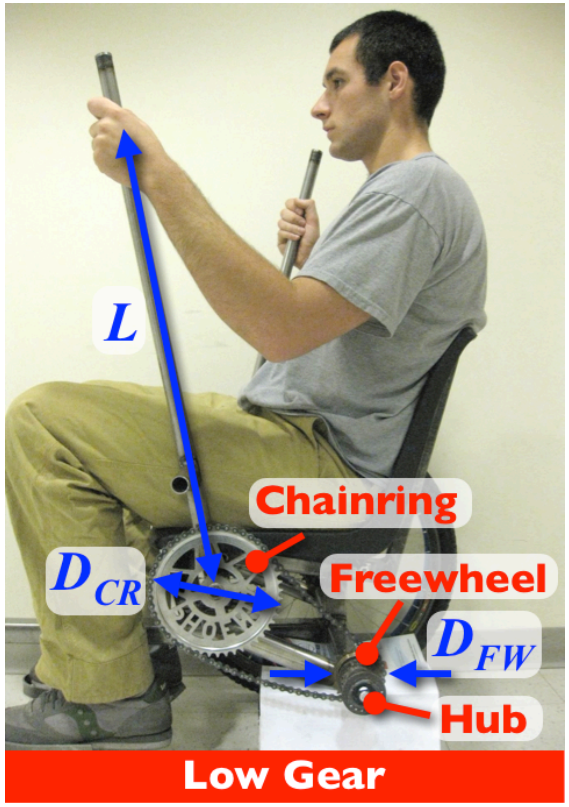

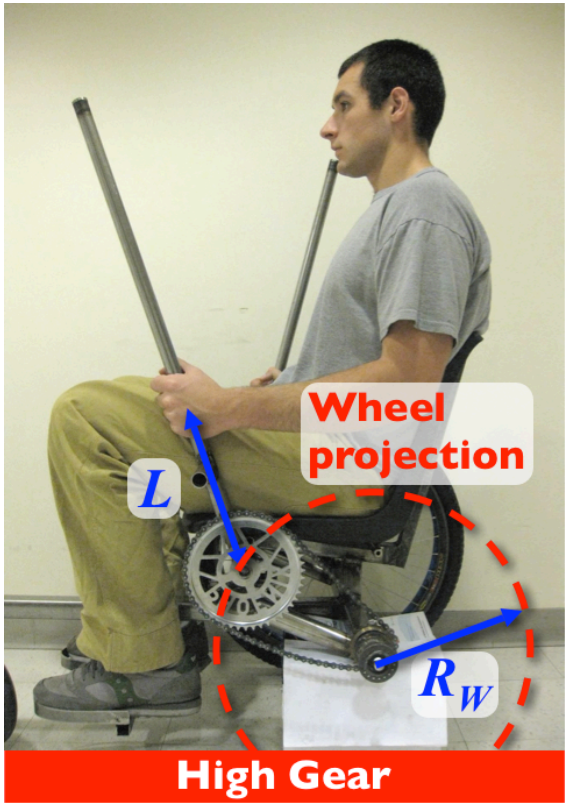

Drivetrain performance

Difference b/w chair velocity (V_{Chair}) and hand velocity (V_{Hand})

$$\frac{V_{Chair}}{V_{Hand}} = \frac{D_{CR} R_W}{D_{FW} L}$$

LFC drivetrain in action

LFC performance capabilities

LFC performance capabilities

Local material construction

- 2X Bottom brackets
- Chainring
- Chain
- Freewheel

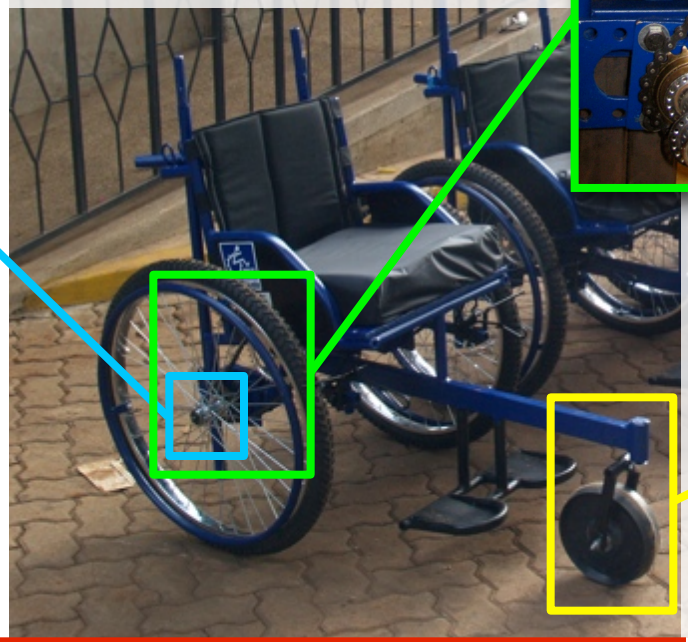

- Rear bike hub
- 1” electrical conduit
- 1/2”, schedule 40 water pipe
- bottom bracket axle

- Front bike hub
- Bottom bracket
- Crank arm

LFC price ≈ $100US
≤ existing wheelchairs

Power of stakeholder input

2008

2009

Power of stakeholder input

2010

LFC project status

JAIPURFOOT.ORG

Pinnacle Industries Ltd.

भारतीय प्रौद्योगिकी संस्थान दिल्ली
INDIAN INSTITUTE OF TECHNOLOGY DELHI

- **Collaborating with Jaipur Foot, Pinnacle Industries, and IIT Delhi**
- **25 chair pre-production trial in India**
- **Commitment from Pinnacle to tool up for 1000 LFCs/month following trial**

LFC project status

Emerging markets + academia

- Opportunity to solve technical problems that affect millions if not *billions* of people
- Facilitate resurgence in US industry by helping it engage emerging markets
- Our duty as educators to prepare our students as Global Engineers

Good science in big problems

Example Problems	Research Solutions
• 1.1 billion people lack clean water[1]	• Physics behind filtration in nature, industry • Low-cost filtration and treatment systems
• 2.5 billion people are forced to use biomass for cooking fuel • Indoor air pollution kills 1.5 million annually[2]	• Particle ablation combustion, heat transfer of cooking • Low-cost charcoal-less biofuel appliances

1. *United Nations Human Development Report*, UNDP, 2006
2. *Human Development Report*, UNDP, 2007

US industry+emerging markets

- BRIC countries forecasted to grow from 18% market capital now to 41% by 2030[1]
- China and India to be first and third largest economies, respectively, by 2050[2]

[1] T. Moe, C. Maasry, and R. Tang. Global Economics Paper No. 204, EM Equity in Two Decades: A Changing Landscape. Technical report, Goldman Sachs, 2010.
[2] J. O'Neill. *BRICs and Beyond*. Goldman Sachs Global Economics Group, 2007.

US industry+emerging markets

Punchline

- Billion+ new middle class consumers
- Billion+ <$4/day consumers who can leverage technology to get out of poverty
- Academics can be an intermediary, linking US industry with emerging markets through research
- US industry funds emerging market research

“Affordable” tech at all levels

Low-cost, portable ultrasound machine[1]

>$100k

<$15k

- Developed in China for China
- Opened new market in US
- Cross-cultural tech transfer!

1. “How GE is Disrupting Itself,” *Harvard Business Review*, 2009

Training global engineers

- Students will have to integrate into a dynamically changing global market place
- Understand local consumer preferences and practices
- Innovate with local talent globally in myriad contexts

Global engineer career track

D-Lab

ENGINEERS WITHOUT BORDERS USA

Harry O'Hanley
MIT BSME 2011
Working in Kenya

"Frontline" experience

Danielle Zurovcik
MIT MSME 2007
Low-Cost Suction Wound Healer

Scientific and engineering rigor

Industry

Amos Winter
Emerging Market Researcher

Academia

IDE

International Development Enterprises

Social entrepreneur

College | Grad student | Professional